SISSA - SCUOLA
INTERNAZIONALE
SUPERIORE
STUDI AVANZATI
TRIESTE
Strada Costiera 11

ISAS - INTERNATIONAL SCHOOL FOR ADVANCED STUDIES

Thesis submitted for the degree

of

"MAGISTER PHILOSOPHIAE"

TOTAL ENERGY MINIMIZATION and AB-INITIO MOLECULAR DYNAMICS SIMULATIONS APPLICATION TO LIQUID AND AMORPHOUS SILICON

CANDIDATE:

I. ŠTICH

SUPERVISORS:

Prof. R. CAR

Prof. M. PARRINELLO

Academic Year 1986/87

TRIESTE

I would like to express my gratitude to my supervisors Profs. R.Car and M.Parrinello for their assistance throughout this work, as well as their help in the preparation of this manuscript.

TOTAL ENERGY MINIMIZATION
and
AB-INITIO MOLECULAR DYNAMICS SIMULATIONS
APPLICATION TO LIQUID AND AMORPHOUS SILICON

Contents

1. Introduction 3

2. Ab-Initio Total Energy Minimization 5

2.1 Total Energy Minimization With Respect to Electronic Degrees of Freedom 13

2.2 Total Energy (Downhill) Minimization With Respect to Ionic Positions 27

2.3 Dynamical Simulations of the Ionic System 31

3. Amorphous and Liquid States From Topological Viewpoint
An Application to Amorphous and Liquid Silicon 38

3.1 Topological Properties of a-Si 44

3.2 Topological Properties of l-Si 49

4. Conclusions 56

References 58

Chaper 1
INTRODUCTION

In this work we report some of our results that have been achieved during the second year of PhD. study in Trieste. Formally, the work is divided in two main parts (chapters 2 and 3), followed by conclusions, given in chapter 4.

Chapter 2 deals mainly with what has become known as the "Car-Parrinello method", i.e. the ab-initio total energy minimization and the ab-initio molecular dynamics formulated in the density functional formalism in the local density approximation. However, unlike the original Car-Parrinello's formulation, we are here more interested in minimization, rather than dynamics, since there is a broad class of physically interesting problems that can be formulated entirely as minimization problems. One of those problems is the standard electronic structure problem for fixed ionic positions. There is now a considerable current interest in solving this problem by using methods that don't require any matrix diagonalization. Our main contribution in this part is in developing a new and efficient minimization method for solving the standard electronic structure problem based on the conjugate gradient strategy. Another important point tackled in this part concerns the ab-initio calculation of forces on ions. We demonstrate and give also some explanation that there is basically only one efficient way of calculating first-principle forces on ions for use in dynamical simulations.

In chapter 3 we attempt at a topological analysis of models of amorphous and liquid silicon generated by methods described in chapter 2. We stress the importance of "oddness" in disordered media. In particular, we carried out a careful ring- and dihedral angle-statistics. These results give the topological characteristics of our models. For the liquid silicon we try to separate the packing and vibration effects thus making a first step towards obtaining the inherent structure of liquid silicon. Since this important aspect of random systems cannot, in principle, be directly

studied by experimental methods, we hope that our first-principle approach can offer a new insight in this old, but not yet fully understood field.

Chaper 2

AB INITIO TOTAL ENERGY MINIMIZATION

This part is a relatively self-contained description of several methods that can be used to calculate the ab-initio total energy minimization in condensed matter systems. A number of our modifications and comments are given to make the methods more powerful.

Within the Hohenberg-Kohn-Sham density functional (DF) formalism [1],[2] the total energy of a solid for a given nuclear configuration is a unique functional of the electronic density $n(\mathrm{r})$. If we express $n(\mathrm{r})$ in terms of occupied single-particle orbitals, i.e.

$$n(\mathrm{r}) = \sum_{i}^{occ} |\psi_i(\mathrm{r})|^2 \tag{2.1}$$

then the total energy is given as the minimum with respect to $\{\psi_i\}$ of the functional

$$E\left[\{\psi_i\},\{\mathbf{R}_I\}\right] = \sum_{i}^{occ} \int_{\Omega} d\mathrm{r}\psi_i^*(\mathrm{r})(-\frac{1}{2}\nabla^2)\psi_i(\mathrm{r}) + U\left[n(\mathrm{r}),\{\mathbf{R}_I\}\right] \tag{2.2a}$$

where $\{\mathbf{R}_I\}$ are the nuclear coordinates and the Kohn-Sham (KS) potential energy U is given by

$$U = \int_{\Omega} V^{ext}(\mathrm{r})n(\mathrm{r})d\mathrm{r} + \frac{1}{2}\int_{\Omega}\frac{n(\mathrm{r})n(\mathrm{r}')}{|\mathrm{r}-\mathrm{r}'|}d\mathrm{r}d\mathrm{r}' + E^{xc}[n] + \frac{1}{2}\sum_{I\neq J}\frac{Z_I Z_J}{|\mathbf{R}_I - \mathbf{R}_J|} \tag{2.2b}$$

In (2.2b) V^{ext} is the external potential felt by the electrons, $E^{xc}[n]$ is the exchange-correlation energy, and Z_I is the nuclear charge.

The global minimum of the functional (2.2) with respect to both nuclear and electronic degrees of freedom gives the stable ground-state configuration of a condensed matter system. From the nature of this problem it is clear that one has to optimize a function depending on a very large number of parameters. There are two cases to be distinguished; namely the local minimum and the global minimum optimization.

Kirkpatrik,Gelatt,and Vecchi [3] showed recently how the concept of simulated annealing can be applied in the latter case. They found a deep connection between statistical mechanics and combinatorial optimization, i.e. finding the minimum of a given function -called objective or cost function $f[\{x_i\}]$- which depends on many parameters $\{x_i\}$. At the heart of the method is an analogy with thermodynamics, specifically the way in which liquids freeze and crystallize (thus finding the minimum energy state) or metals cool and anneal.

Metropolis Monte-Carlo (MC) [4] algorithm, whose acceptance probability for a given configuration is defined as the Boltzmann probability distribution

$$p = \exp\left(\frac{-\Delta E}{k_B T}\right) \tag{2.3}$$

provides a simple algorithm for simulating the equilibrium configurations of atoms in contact with a heat bath at temperature T. Using the cost function in place of the energy the Metropolis procedure generates a population of configurations in a given optimization problem at some effective temperature. This temperature serves as a control parameter. In the simulated annealing process the system being optimized is first "melted" at a high T, then the temperature is lowered slowly until for $T \rightarrow 0$ the system "freezes" in the minimum. If the cooling process is slow enough, the minimum reached will be the global one. Otherwise, if $f[\{x_i\}]$ has several closely spaced minima, one of these almost degenerate states will be reached. The gross rearrangements in the objective function occur at high T, while small changes take place at low T. This is so because at high T one samples much larger region of the parameter space. The temperature keeps the algorithm from getting stuck in a local minimum by permitting uphill moves.

It is possible to use the simulated annealing technique to minimize the DF functional (2.2). Having the temperature of the system under control not only enables the global minimization of (2.2), but by varying this temperature it is also possible to let the system undergo various thermal treatments, such as annealing and quenching. Since the nature of interactions involved in (2.2) is not short-ranged

and the KS orbitals $\{\psi_i\}$ are subject to holonomic orthogonality constraints

$$\int_\Omega d\mathbf{r}\psi_i^*(\mathbf{r})\psi_j(\mathbf{r}) = \delta_{ij}$$

the molecular dynamics (MD), rather then MC method is better suited to minimize the energy functional (2.2). Following Car and Parrinello's formulation [5] one can introduce a classical dynamical system defined by the Lagrangean:

$$L = \int dr \sum_i \frac{1}{2} M_i |\dot{\psi}_i|^2 + \sum_I \frac{1}{2} M_I \dot{\mathbf{R}}_I^2 - E\left[\{\psi_i\}, \{\mathbf{R_I}\}\right] + \sum_{ij} \Lambda_{ij} \left(\int dr \psi_i^* \psi_j - \delta_{ij} \right) \tag{2.4}$$

where $\{M_i\}$ are fictitious masses associated with the dynamics of the electronic wavefunctions, $\{M_I\}$ are the physical ionic masses and Λ is an hermitian matrix of Lagrangean multipliers imposing the orthogonality constraints on the KS orbitals $\{\psi_i\}$. In the dynamical system defined by (2.4) the KS functional plays the role of the potential energy.

The Lagrange equations-of-motion

$$\frac{d}{dt}\left(\frac{\delta L}{\delta \dot{\psi}_i^*}\right) = \frac{\delta L}{\delta \psi_i^*} \tag{2.5a}$$

$$\frac{d}{dt}\left(\frac{\partial L}{\partial \dot{\mathbf{R}}_I}\right) = \frac{\partial L}{\partial \mathbf{R}_I} \tag{2.5b}$$

generate the fictitious dynamics for $\{\psi_i\}$ and the real dynamics for $\{\mathbf{R}_I\}$ through the equations-of-motion:

$$M_i \ddot{\psi}_i(\mathbf{r}, t) = -\frac{\delta E}{\delta \psi_i^*(\mathbf{r}, t)} + \sum_k \Lambda_{ik} \psi_k(\mathbf{r}, t) \tag{2.6a}$$

$$M_I \ddot{\mathbf{R}}_I = -\nabla_{\mathbf{R}_I} E \tag{2.6b}$$

The classical kinetic energy of the dynamical system is

$$K = \sum_i \frac{1}{2} M_i \int dr |\dot{\psi}_i|^2 + \sum_I \frac{1}{2} M_I \dot{\mathbf{R}}_I^2 \tag{2.7}$$

Its average is related to the temperature of the system. Reducing slowly this temperature the equilibrium state of minimal E can be reached for $T \to 0$. Thus one obtains in the MD context the same objective of the simulated annealing, as in MC.

Eq. (2.6b) may also be used to generate ab-initio Born-Oppenheimer (BO) dynamics of the ionic subsystem. The condition for the validity of the BO dynamics is that the electronic wavefunctions are always in the ground-state pertinent to the instantaneous ionic configuration. This constraint defines the many-body energy surface $\Phi[\{R_I\}]$ to be sampled by (2.6b) via the condition

$$\Phi[\{\mathbf{R}_I\}] = \min_{\{\psi_i\}} E[\{\psi_i\}, \{\mathbf{R}_I\}] \tag{2.8}$$

Eq. (2.8) can be approximately satisfied by the dynamics generated via eqs. (2.6) if the electronic dynamics proceeds much faster compared to the ionic dynamics. Then the evolution of (2.4) is adiabatic, with no energy transfer between ionic and electronic subsystems. To set up such a regime requires the $\{M_i\}$ to be small compared to $\{M_I\}$ and the $\{\psi_i\}$ to be initially in the ground state. Small $\{M_i\}$ in turn require a small time step in the numerical integration of the differential equations (2.6), what means that the adiabatic dynamics may be costly. This raises the question whether the dynamics described by (2.6) is the optimal one. An alternative dynamics could be generated by decoupling the electronic and ionic motions and using directly eq. (2.8) by performing a separate electronic minimization for any time step. Both types of dynamics will be analyzed in detail in section 2.3 .

A different situation arises when one is interested only in mapping the system onto a local minimum of a potential function in a downhill manner. This is the case when one needs to speed up the convergence close to the desired minima or for an efficient mapping of the system onto a nearby minimum (like in calculation of the inherent structure [49]) and in many other purely local minimization problems. Particularly relevant in this context is the problem of finding the electronic ground-state for a fixed ionic configuration, as defined by (2.8). In fact, experience has shown that for fixed ionic configuration the energy density functional, in the approximations commonly used, has a single minimum [6],[7],[8],[9]. This makes the use of minimization procedures tailored to handle the multiminimum problems, such as simulated annealing, rather inconvenient. We have therefore explored the possibility of applying more conventional minimization methods. The downhill min-

imization with respect to the electronic degrees of freedom is an efficient procedure, provided we start from an initial electronic configuration having the right symmetry and the initial and final states are not orthogonal. This point is in detail addressed in section 2.1.

The most naive idea in this case is to replace the dynamical second-order Newton's eqs. (2.6) by the corresponding first-order equations:

$$M_i\dot{\psi}_i(\mathbf{r},t) = -\frac{\delta E}{\delta \psi_i^*(\mathbf{r},t)} + \sum_k \Lambda_{ik}\psi_k(\mathbf{r},t) \tag{2.9a}$$

$$M_I\dot{\mathbf{R}}_I = -\nabla_{\mathbf{R}_I} E \tag{2.9b}$$

Eqs. (2.9) are equations of *steepest descent* (SD) type and define a mass weighted SD trajectory on the E surface moving downhill to a nearby minimum. Eqs. (2.9) are equivalent to eqs. (2.6) if the temperature $T = 0$ is kept in the MD equations (no uphill moves are permitted). This can most easily be seen in discretized form. Eqs. (2.6) have the following general form:

$$M\ddot{x}(t) = F(t) \tag{2.10}$$

where M is the mass pertaining to the dynamical variable x, and F is the force acting on x. Eq. (2.10) discretized according to the Verlet algorithm [10] reads

$$\begin{aligned} x(t+\Delta t) &= x(t) + \Delta t\dot{x}(t) + \frac{\Delta t^2}{2}\ddot{x}(t) + \cdots \\ &= -x(t-\Delta t) + 2x(t) + \frac{\Delta t^2}{M}F(t) + O(\Delta t^4) \end{aligned} \tag{2.11}$$

If the condition $T = 0$, and consequently also $\dot{x} = 0$, is imposed, eq. (2.11) becomes

$$x(t+\Delta t) = x(t) + \frac{\Delta t^2}{2M}F(t) \tag{2.12}$$

which can be interpreted as a discretized form of the eq. of the type (2.9), once the time step Δt is properly scaled.

We now briefly illustrate some minimization methods that will be used in the following. Let us suppose that the function to be minimized is roughly approximated

as a quadratic form around some point P taken as the origin of the coordinate system:

$$f(X) \approx c - \langle b, X\rangle + \frac{1}{2}\langle X, AX\rangle \tag{2.13}$$

where

$$c \equiv f(P) \quad ; \quad b \equiv -\nabla f|_P \quad ; \quad A_{ij} \equiv \frac{\partial^2 f}{\partial x_i \partial x_j}|_P \tag{2.14}$$

with a symmetric positive definite (SPD) $N \times N$ Hessian matrix A.

A broad class of minimization methods in multidimensions is based on sequences of one-dimensional line minimizations. They start from some point P and some vector direction h in N-dimensional space, find the scalar λ that minimizes $f(P + \lambda h)$ and replace P by $P + \lambda h$ etc... Different methods differ only how, at each stage, they chose the next direction h to try. Here we concentrate only on SD *"with adjustable steps"* and *conjugate gradient* (CG) methods [11]. As far as we know, the other methods don't have any overwhelming advantages over CG.

The most natural choice for h is $-\nabla f = F$ (the force) what leads in the approximation (2.13),(2.14) to:

$$P_{n+1} = P_n + \lambda_n h_n \quad ; \quad n = 0, 1, 2 \cdots \tag{2.15}$$

$$h_n = b - AP_n$$

where λ_n is chosen to minimize $f(P_{n+1})$, i.e.

$$\lambda_n = \frac{\langle h_n, h_n\rangle}{\langle h_n, Ah_n\rangle} = \frac{\langle F_n, F_n\rangle}{\langle F_n, AF_n\rangle}$$

It is easily seen that (2.12) and (2.15) are equivalent apart from the factor multiplying the force in (2.12). Algorithm of type (2.15) will be referred to as SD "with adjustable steps".

The problem with SD is that the new gradient at the minimum point of any line minimization is often nearly perpendicular to the direction just traversed. Therefore SD will perform many small right-angled steps going downhill, what renders SD as

rather inefficient. SD is particularly inefficient when the minimum has a canyon-like shape of the kind illustrated in fig.1.

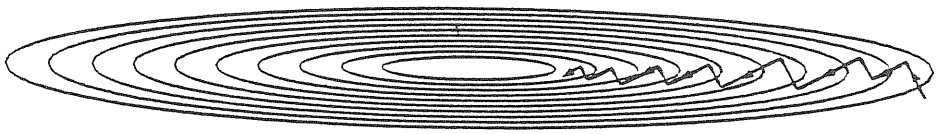

Fig.1. A canyon-like minimum. The SD trajectory is far from the optimal one.

By chosing the direction vectors h wisely, one can reach the minimum in at most N iterations in the absence of rounding errors. This is the case for the CG method. In the CG method one defines two sequences of vectors :

$$\begin{aligned} g_0 &= arbitrary \quad ; \quad h_0 = g_0 \\ g_{n+1} &= g_n - \lambda_n A h_n \quad ; \quad n = 0, 1, 2 \cdots \\ h_{n+1} &= g_{n+1} + \gamma_n h_n \end{aligned} \tag{2.16}$$

where λ_n, γ_n are chosen to make $\langle g_{n+1}, g_n \rangle = 0$ and $\langle h_{n+1}, A h_n \rangle = 0$ i.e

$$\lambda_n = \frac{\langle g_n, g_n \rangle}{\langle g_n, A h_n \rangle} = \cdots = \frac{\langle g_n, h_n \rangle}{\langle h_n, A h_n \rangle}$$

$$\gamma_n = -\frac{\langle g_{n+1}, A h_n \rangle}{\langle h_n, A h_n \rangle} = \cdots = \frac{\langle g_{n+1}, g_{n+1} \rangle}{\langle g_n, g_n \rangle}$$

Then $\forall m \neq n$

$$\begin{aligned} \langle g_n, g_m \rangle &= 0 \quad - orthogonality \\ \langle h_n, A h_m \rangle &= 0 \quad - conjugacy \end{aligned} \tag{2.17}$$

Thus (2.16), which is a kind of Gram-Schmidt bi-orthogonalization produces a sequence of g's that are all mutually orthogonal and a sequence of h's that are all

mutually conjugate. The calculation of A, required to construct the g's can be avoided using the following theorem: Let $g_n = -\nabla f(P_n)$ for some P_n,where f is of the form (2.13). Then we proceed from P_n along direction h_n to the local minimum of f located at P_{n+1} and then set $g_{n+1} = -\nabla f(P_{n+1})$. Then g_{n+1} is the same as that given by (2.16). Indeed, if f is of the form (2.13) we have $g_n = b - AP_n$ and

$$g_{n+1} = b - A(P_n + \lambda_n h_n) = g_n - \lambda_n A h_n$$

$$\langle g_{n+1}, h_n \rangle = \langle g_n, h_n \rangle - \lambda_n \langle h_n, A h_n \rangle$$

At the minimum $h_n.\nabla f = -h_n.g_{n+1} = 0$ and

$$\lambda_n = \frac{\langle g_n, h_n \rangle}{\langle h_n, A h_n \rangle}$$

and so g_{n+1} is identical to g_{n+1} from (2.16). Note that this proof explicitly uses the fact that f is of the form (2.13) and that only the direction of h, not the orientation is important in this proof.

Summing up, one finds the following CG algorithm

$$\begin{aligned} P_{n+1} &= P_n + \lambda_n h_n \quad ; \quad n = 0, 1, 2 \cdots \\ h_n &= \begin{cases} g_n & \text{n=0} \\ g_n + \gamma_{n-1} h_{n-1} & \text{n=1,2,3} \cdots \end{cases} \\ g_n &= b - AP_n (= g_{n-1} - \lambda_n A h_{n-1}) \quad ; \quad n = 0, 1, 2 \cdots (n = 1, 2, 3 \cdots) \end{aligned} \tag{2.18}$$

We will specify this minimization technique to the case of the energy density functional (2.2) in sections 2.1 and 2.2. In section 2.1 the ionic coordinates are kept fixed, while in section 2.2 the more general problem of minimizing also with respect to the ionic positions will be briefly discussed.

2.1 TOTAL ENERGY MINIMIZATION WITH RESPECT TO ELECTRONIC DEGREES OF FREEDOM

In this section methods for solving the standard electronic structure problem for a fixed ionic configuration based on simulated annealing MD and iterative downhill minimization will be introduced, discussed and compared with some non-standard diagonalization techniques. This is an important point because there is much current interest in methods that don't involve straight matrix diagonalization. Particular attention will be given to the extension of the CG method [12] to the electronic minimization, since this method was found to be the most efficient.

Here we suppose to deal with a periodic solid even though the periodicity may be an artificial consequence of using the supercell method (the case of amorphous solids, liquids, single defect, crystal surface calculations etc.). In this case Bloch theorem holds and the wavefunctions can conveniently be expanded in a plane wave basis set :

$$\psi_{i,\mathbf{k}}(\mathbf{r}) = \sum_{\mathbf{G}} c_{i,\mathbf{k}+\mathbf{G}} \exp\{i(\mathbf{k}+\mathbf{G}).\mathbf{r}\} \qquad (2.1.1)$$

where the $\mathbf{G}$'s are the reciprocal lattice vectors, and $\mathbf{k}$ lies in the first Brillouin zone (BZ). Although not strictly necessary, we find convenient to use the following approximations. We suppose that the core electrons have been removed and the strong ionic potential replaced by a weaker pseudopotential acting on the pseudo-wavefunctions rather than the true valence functions. The pseudopotential approximation not only largely reduces the number of states to be dealt with, but also the number of plane waves, since the pseudopotential is much weaker than the true ionic potential. We also suppose that the exchange and correlation is treated at the local density approximation (LDA) [1] level.

In the standard approach one solves the KS equations

$$\left[-\frac{1}{2}\nabla^2 + V^{ion}(\mathbf{r}) + V^{H}(\mathbf{r}) + V^{xc}(\mathbf{r})\right]\psi_{i,\mathbf{k}}(\mathbf{r}) = \lambda_{i,\mathbf{k}}\psi_{i,\mathbf{k}}(\mathbf{r}) \qquad (2.1.2a)$$

$$H\psi_{i,\mathbf{k}}(\mathbf{r}) = \lambda_{i,\mathbf{k}}\psi_{i,\mathbf{k}}(\mathbf{r})$$

where V^{ion} is the ionic potential, $\lambda_{i,\mathbf{k}}$ are the KS eigenvalues, V^H is the Hartree potential, and V^{xc} is the exchange-correlation potential. The latter two quantities depend on the electronic density and have to be determined self-consistently. In the plane wave basis one solves for the expansion coefficients $c_{i,\mathbf{k}+\mathbf{G}}$ from eq. (2.1.1), which are solutions to

$$\frac{1}{2}|\mathbf{k}+\mathbf{G}|^2 c_{i,\mathbf{k}+\mathbf{G}} + \sum_{\mathbf{G}'} V^H_{\mathbf{G}-\mathbf{G}'} c_{i,\mathbf{k}+\mathbf{G}'} + \sum_{\mathbf{G}'} V^{xc}_{\mathbf{G}-\mathbf{G}'} c_{i,\mathbf{k}+\mathbf{G}'}$$

$$+ \sum_{\mathbf{G}'} V^{ion}_{\mathbf{k}+\mathbf{G},\mathbf{k}+\mathbf{G}'} c_{i,\mathbf{k}+\mathbf{G}'} = \lambda_{i,\mathbf{k}} c_{i,\mathbf{k}+\mathbf{G}} \qquad (2.1.2b)$$

The electronic density n(r) is given as

$$n(\mathbf{r}) = \sum_{i}^{occ} \int_{BZ} d\mathbf{k} |\psi_{i,\mathbf{k}}(\mathbf{r})|^2 \qquad (2.1.3)$$

In semiconductors the sum over the BZ can be carried out very accurately by summing only over few special k points [13]. Eqs. (2.1.2b), (2.1.3) have to be solved self-consistently.

Suppose now that N electronic states are expanded in M plane waves. The standard diagonalization of the matrix H requires M^3 operations for each k point and has to be done I times to iterate to self-consistency. Thus the standard diagonalization techniques require on the order of IM^3 operations.

If all the potentials in (2.1.2a) were correct the density (2.1.3) would be the correct density that minimizes the true KS functional and the $\lambda's$ would be the lower bounds for the variational expectation values of H for any trial wavefunction ψ . Let λ_1 be the lowest energy eigenstate and ψ_1 be a corresponding trial wavefunction. Then

$$\langle \psi_1, H\psi_1 \rangle \geq \lambda_1 \qquad (2.1.4)$$

If ψ_1 is expanded in some orthonormal basis set $\{\Phi_n\}$, (2.1.4) gives the following condition :

$$\sum_{m,n} c^*_m c_n \langle \Phi_m, H\Phi_n \rangle \geq \lambda_1 \qquad (2.1.5)$$

subject to the normalization constraint

$$\sum_n |c_n|^2 = 1 \tag{2.1.6}$$

Thus by varying c_n in (2.1.5), (2.1.6) and minimizing the left-hand-side of (2.1.5) gives an upper bound to the lowest-energy value of H. The same procedure can be repeated also for the higher eigenstates if one imposes the orthogonality to the lower energy eigenfunctions. These eigenstates would be identical to those obtained by standard diagonalization procedure and the electronic density calculated using these eigenstates would minimize the KS functional E, and would give the corresponding point on the BO surface defined in (2.8). There are several methods (besides standard diagonalization) to find the combination of expansion coefficients that minimizes the KS energy functional. Car and Parrinello's original approach [5] was formulated entirely in the language of MD and simulated annealing. The dynamical eqs. of motion for the KS orbital (2.6a) are :

$$M_i \ddot{\psi}_{i,\mathbf{k}}(\mathbf{r},t) = -H\psi_{i,\mathbf{k}}(\mathbf{r},t) + \sum_j \Lambda_{ij,\mathbf{k}}\psi_{j,\mathbf{k}}(\mathbf{r},t) \tag{2.1.7}$$

Equivalent formulation for the expansion coefficients in the plane wave basis set gives :

$$M_i \ddot{c}_{i,\mathbf{k}+\mathbf{G}} = -\frac{1}{2}|\mathbf{k}+\mathbf{G}|^2 c_{i,\mathbf{k}+\mathbf{G}} - \sum_{\mathbf{G}'} V^H_{\mathbf{G}-\mathbf{G}'} c_{i,\mathbf{k}+\mathbf{G}'} - \sum_{\mathbf{G}'} V^{xc}_{\mathbf{G}-\mathbf{G}'} c_{i,\mathbf{k}+\mathbf{G}'}$$

$$- \sum_{\mathbf{G}'} V^{ion}_{\mathbf{k}+\mathbf{G},\mathbf{k}+\mathbf{G}'} c_{i,\mathbf{k}+\mathbf{G}'} + \sum_j \Lambda_{ij,\mathbf{k}} c_{j,\mathbf{k}+\mathbf{G}} \tag{2.1.8a}$$

Discretized according to the Verlet algorithm [10] this equation reads

$$c_{i,\mathbf{k}+\mathbf{G}}(t+\Delta t) = -c_{i,\mathbf{k}+\mathbf{G}}(t-\Delta t) + 2c_{i,\mathbf{k}+\mathbf{G}}(t) + \Delta t^2 \ddot{c}_{i,\mathbf{k}+\mathbf{G}}(t) + O(\Delta t^4) \tag{2.1.8b}$$

Verlet algorithm is a low order integration formula, that however has minimal storage requirements on the coefficients c.

Since the starting wavefunctions are not the self-consistent KS orbitals, the KS energy functional is not minimized and the system has some available potential

energy. On integration, the coefficients begin to move and a part of the potential energy will be converted to kinetic energy. Reducing the temperature will remove some fictitious kinetic energy from the system. In an attempt to re-establish equipartition, potential energy will be converted to kinetic energy until all the excess potential energy is removed at $T \to 0$. At equilibrium $\{\ddot{\psi}_{i,\mathbf{k}+\mathbf{G}}\} = 0$ and the electronic states become within a unitary transformation the self-consistent solutions to the KS eqs.

Since the potential is updated at each step, the electronic states at the end of the minimization process will automatically be eigenstates of the self-consistent Hamiltonian H. The iterative improvement combined with automatical obtaining of self-consistency is an important feature not present in standard diagonalization techniques.

This procedure requires for each k point on the order of $INM \ln M$ and IN^2M operations [5]. Since usually $N \ll M$, each step is significantly less computationally demanding compared to traditional diagonalization techniques. However I, the number of time steps necessary to converge the calculation in the MD method is larger than the number of iterations necessary for self-consistency in matrix diagonalization methods. So the MD method in this form usually doesn't provide a significant improvement over the matrix diagonalization.

The number of iterations I is the key to make this class of methods efficient. Since it appears that there is only a single minimum and no barriers to climb up [6],[7],[8],[9], downhill minimization methods should do in this context a better job, reducing I significantly.

If we specialize the SD eq. to the problem of electronic minimization we find eq. (2.9a)

$$M_i \dot{\psi}_{i,\mathbf{k}}(\mathbf{r},t) = -H\psi_{i,\mathbf{k}}(\mathbf{r},t) + \sum_j \Lambda_{ij,\mathbf{k}}\psi_{j,\mathbf{k}}(\mathbf{r},t) \qquad (2.1.9a)$$

or in discretized form in the space of the plane wave coefficients

$$c_{i,\mathbf{k}+\mathbf{G}}(t+\Delta t) = c_{i,\mathbf{k}+\mathbf{G}}(t) + \frac{\Delta t^2}{2}\dot{c}_{i,\mathbf{k}+\mathbf{G}}(t) \qquad (2.1.9b)$$

The number of operations required is as before $IMN \ln M$ and IN^2M, however I

is now greatly reduced.

There was an attempt to reduce I by using a modified integration scheme for eqs. (2.1.7),(2.1.8). This method will be referred to as Payne, Joannopoulos,Allan, Tetter, Vanderbilt (PJATV) algorithm [14]. On replacing $\Lambda_{ij,\mathbf{k}}$ by its diagonal part $\lambda_{i,\mathbf{k}}$ and separation the diagonal terms, the equation (2.1.8a) becomes

$$M_i\ddot{c}_{i,\mathbf{k}+\mathbf{G}} = -\left[\frac{1}{2}|\mathbf{k}+\mathbf{G}|^2 + V_{\mathbf{G}'=\mathbf{G}} - \lambda_{i,\mathbf{k}}\right] c_{i,\mathbf{k}+\mathbf{G}} - \sum_{\mathbf{G}'\neq\mathbf{G}} V_{\mathbf{k}+\mathbf{G},\mathbf{k}+\mathbf{G}'}c_{i,\mathbf{k}+\mathbf{G}'} \tag{2.1.10}$$

If we identify :

$$\omega^2 = \left[\frac{1}{2}|\mathbf{k}+\mathbf{G}|^2 + V_{\mathbf{G}'=\mathbf{G}} - \lambda_{i,\mathbf{k}}\right] M_i^{-1}$$

$$R = \left[\sum_{\mathbf{G}'\neq\mathbf{G}} V_{\mathbf{k}+\mathbf{G},\mathbf{k}+\mathbf{G}'}c_{i,\mathbf{k}+\mathbf{G}'}\right] M_i^{-1}$$

eq. (2.1.10) can be rewritten as

$$\ddot{c}_{i,\mathbf{k}+\mathbf{G}} = -\omega^2 c_{i,\mathbf{k}+\mathbf{G}} - R \tag{2.1.11}$$

Eq. (2.1.11) is basically an oscillator equation. An analytic integration of this equation gives

$$c_{i,\mathbf{k}+\mathbf{G}}(t+\Delta t) = -c_{i,\mathbf{k}+\mathbf{G}}(t-\Delta t) + 2\cos(\omega\Delta t)c_{i,\mathbf{k}+\mathbf{G}}(t) - 2\left[1-\cos(\omega\Delta t)\right]R\omega^{-2} \tag{2.1.12}$$

A similar procedure can be followed also for the SD eq. [6],[7]. In such a case the integration algorithm reads

$$c_{i,\mathbf{k}+\mathbf{G}}(t+\Delta t) = \exp(-\omega^2\Delta t)c_{i,\mathbf{k}+\mathbf{G}}(t) - R\omega^{-2} \tag{2.1.13}$$

The usefulness of these two approaches can be explained as follows. If one uses the Verlet algorithm to integrate the equations, the largest time step Δt is restricted by the plane waves that have the highest kinetic energy (because ω increases with G) and are the least important contributions to the wavefunctions. This limitation is partially alleviated by performing an analytic integration. In these approaches,

instead, the value of Δt is limited by the largest time step that can be taken before updating R in (2.1.12),(2.1.13). This limitation will not be severe if the Hamiltonian matrix is diagonally dominated and R is a relatively small perturbation. From our numerical results it will be clear that this is not always the case and that the presence of structural disorder plays an important role in performance of these methods. So the PJATV doesn't appear as an integration scheme which is generally convenient.

Rather than elaborating on a better integration scheme of SD type of equations it seems better to adopt an altogether different minimization scheme. As already anticipated, the CG might be a good choice [12]. However, the standard CG method cannot be used as it stands since our minimization problem is constrained by the orthogonality requirement. We will show below how this constraint can be incorporated in a practical way into the CG scheme. There are two important ingredients of CG as summarized in (2.18); namely the calculation of constrained forces and the line minimization in the direction of h.

As is evident from (2.1.7) the forces acting on the KS orbitals have two components: forces arising from action of the Hamiltonian and forces of constraint. These forces of constraints must be taken into account when the line minimizations are done. In order to avoid multiple reorthogonalizations let us now reformulate eq. (2.1.7) in terms of linearly independent but not orthonormal orbitals $\{\varphi_i\}$. The orthonormal orbitals $\{\psi_i\}$ can be related to the $\{\varphi_i\}$ via

$$\psi_i = \sum_j S_{ij}^{-\frac{1}{2}} \varphi_j \tag{2.1.14}$$

where

$$S_{ij} = \langle \varphi_j, \varphi_i \rangle \tag{2.1.15}$$

is the overlap matrix.

All the principal quantities can be formulated in terms of the non-orthonormal orbitals $\{\varphi_i\}$, e.g. the particle density n(r) is given by :

$$n(\mathbf{r}) = \sum_l^{occ} \psi_l^*(\mathbf{r})\psi_l(\mathbf{r}) = \sum_{ijl}^{occ} S_{il}^{-\frac{1}{2}} \varphi_i^*(\mathbf{r}) S_{lj}^{-\frac{1}{2}} \varphi_j(\mathbf{r}) = \sum_{ij}^{occ} \varphi_i^*(\mathbf{r}) S_{ij}^{-1} \varphi_j(\mathbf{r}) \tag{2.1.16}$$

or the KS functional

$$E = \sum_{l}^{occ} \langle \psi_l | H | \psi_l \rangle = \sum_{lij}^{occ} \int dr S_{il}^{-\frac{1}{2}} \varphi_i^*(\mathrm{r}) H S_{lj}^{-\frac{1}{2}} \varphi_j(\mathrm{r}) = \sum_{ij}^{occ} S_{ij}^{-1} \langle \varphi_i, H\varphi_j \rangle \quad (2.1.17)$$

Instead of minimizing the KS functional with respect to $\{\psi_i\}$, as in (2.1.7) we can minimize it relative to $\{\varphi_i\}$

$$M_l \ddot{\varphi}_l(\mathrm{r},t) = -\frac{\delta}{\delta \varphi_l^*(\mathrm{r},t)} \sum_{ij}^{occ} S_{ij}^{-1} \langle \varphi_i(\mathrm{r},t), H\varphi_j(\mathrm{r}) \rangle$$

$$= -\left[\sum_{j}^{occ} S_{lj}^{-1} H\varphi_j(\mathrm{r},t) + \sum_{lj}^{occ} \frac{\delta S_{ij}^{-1}}{\delta \varphi_l^*(\mathrm{r},t)} \langle \varphi_i(\mathrm{r},t), H\varphi_j(\mathrm{r},t) \rangle \right] \quad (2.1.18)$$

In order to construct $\frac{\delta S_{ij}^{-1}}{\delta \varphi_l^*(\mathrm{r},t)}$ we can take the derivative of the relation

$$\sum_k S_{mk} S_{kj}^{-1} = \delta_{mj}$$

thus finding

$$\sum_k \left[\frac{\delta S_{mk}}{\delta \varphi_l^*(\mathrm{r},t)} S_{kj}^{-1} + S_{mk} \frac{\delta S_{kj}^{-1}}{\delta \varphi_l^*(\mathrm{r},t)} \right] = 0$$

and

$$\frac{\delta S_{ij}^{-1}}{\delta \varphi_l^*(\mathrm{r},t)} = -\sum_{km} S_{im}^{-1} \frac{\delta S_{mk}}{\delta \varphi_l^*(\mathrm{r},t)} S_{kj}^{-1} = -\sum_m S_{im}^{-1} \varphi_m(\mathrm{r},t) S_{lj}^{-1} \quad (2.1.19)$$

Inserting (2.1.19) into (2.1.18) gives

$$M_l \ddot{\varphi}_l(\mathrm{r},t) = -\left[\sum_j S_{lj}^{-1} H\varphi_j(\mathrm{r},t) - \sum_{ijm} \langle \varphi_i(\mathrm{r},t), H\varphi_j(\mathrm{r},t) \rangle S_{im}^{-1} S_{lj}^{-1} \varphi_m(\mathrm{r},t) \right] \quad (2.1.20)$$

Eq. (2.1.20) is the equivalent of eq. (2.1.7) expressed in terms of non-orthonormal orbitals $\{\varphi_l\}$. From (2.1.20) it is evident that the constrained force acting on the l th KS orbital is

$$F_l(\mathrm{r},t) = -\sum_j S_{lj}^{-1} H\varphi_j(\mathrm{r},t) + \sum_{ijm} \langle \varphi_i(\mathrm{r},t), H\varphi_j(\mathrm{r},t) \rangle S_{im}^{-1} S_{lj}^{-1} \varphi_m(\mathrm{r},t) \quad (2.1.21)$$

For initially orthonormal orbitals (2.1.21) reduces to

$$F_l = -H\varphi_l + \sum_m \langle \varphi_m, H\varphi_l \rangle \varphi_m \qquad (2.1.22)$$

It is advantageous to reorthogonalize the wavefunctions after each CG step. This is a unitary transformation that doesn't influence the results but enables to use the simple formula (2.1.22) and guarantees that the overlap matrix is always well defined.

The CG minimization procedure applied to the minimization of the KS energy functional relative to the wavefunctions $\{\varphi_i\}$ can be summarized as follows

$$\varphi_i^{(n+1)} = \varphi_i^{(n)} + \lambda_n h_i^{(n)} \quad ; \quad n = 0, 1, 2 \cdots$$

$$h_i^{(n)} = \begin{cases} g_i^{(n)} & \text{n=0} \\ g_i^{(n)} + \gamma_{n-1} h_i^{(n-1)} & \text{n=1,2,3}\cdots \end{cases} \qquad (2.1.23)$$

$$g_i^{(n)} = F_i^{(n)} = -H\varphi_i^{(n)} + \sum_m \langle \varphi_m^{(n)}, H\varphi_i^{(n)} \rangle \varphi_m^{(n)} \quad ; \quad n = 0, 1, 2 \cdots$$

$$\gamma_{n-1} = \frac{\sum_{i=1}^N \langle g_i^{(n)}, g_i^{(n)} \rangle}{\sum_{i=1}^N \langle g_i^{(n-1)}, g_i^{(n-1)} \rangle} \quad ; \quad n = 1, 2, 3 \cdots$$

λ_n must be chosen so as to minimize the KS energy functional along the direction h :

$$E(\lambda_n) = \sum_{ij} \langle \varphi_i^{(n+1)}(\mathrm{r}), H\varphi_j^{(n+1)}(\mathrm{r}) \rangle S_{ij}^{-1\ (n+1)} \qquad (2.1.24a)$$

Since we deal with a self-consistent problem the Hamiltonian H should be updated along the direction h. To keep things simple, we fix H in the line minimization and update it only at the minimum of each direction h. This approximation requires computation of the following matrices : $\langle \varphi, H\varphi \rangle$, $\langle \varphi, Hh \rangle + cc$,$\langle h, Hh \rangle$, $\langle \varphi, h \rangle + cc$,$\langle h, h \rangle$, and becomes progressively better when approaching the desired minimum.

Again, as before eqs. (2.1.20)-(2.1.23) can be explicitly written in the plane wave basis set in a manner parallel to eqs. (2.1.8),(2.1.9).

In the above formulation we have labeled the orbitals by a single index. However, in a solid the states are labeled by the band index and the k quantum number. In this case the k label must be added to all the indices in (2.1.23) and (2.1.24) reads as

$$E(\{\lambda_{n,\mathbf{k}}\}) = \int_{BZ} d\mathbf{k} \sum_{ij} \langle \varphi_{i,\mathbf{k}}^{(n+1)}(\mathbf{r}), H\varphi_{j,\mathbf{k}}^{(n+1)}(\mathbf{r})\rangle S_{ij,\mathbf{k}}^{-1\ (n+1)}$$

$$\approx \sum_{\mathbf{k}\in BZ} \sum_{ij} \langle \varphi_{i,\mathbf{k}}^{(n+1)}(\mathbf{r}), H\varphi_{j,\mathbf{k}}^{(n+1)}(\mathbf{r})\rangle S_{ij,\mathbf{k}}^{-1\ (n+1)} \qquad (2.1.24b)$$

The problem of line minimization can thus be decomposed in a number of line minimizations, one for each k point used in the BZ sampling. The vectors φ,h,g become supervectors of the form :

$$\phi = \begin{pmatrix} \{\varphi_{i,\mathbf{k}_1}\} \\ \vdots \\ \{\varphi_{i,\mathbf{k}_{NK}}\} \end{pmatrix} \qquad h = \begin{pmatrix} \{h_{i,\mathbf{k}_1}\} \\ \vdots \\ \{h_{i,\mathbf{k}_{NK}}\} \end{pmatrix} \qquad g = \begin{pmatrix} \{g_{i,\mathbf{k}_1}\} \\ \vdots \\ \{g_{i,\mathbf{k}_{NK}}\} \end{pmatrix} \qquad (2.1.25)$$

respectively (NK being the number of k points used in BZ sampling).

Let us estimate the computational burden of CG for electrons. The main increase compared to SD comes from the necessity to compute not only the action of the Hamiltonian on the wavefunction φ but also on the direction vectors h. This operations scale as IN^2M. To perform the Fourier transforms requires $INM \ln M$ operations. To compute each of the above matrices requires IN^2M operations. NM operations are necessary to compute γ, and N^3 operations to invert the overlap matrix S. Since $N \ll M$ the number of operations in the CG scales as IN^2M with a prefactor slightly more than doubled compared to SD. However the number of iterations necessary to converge the calculation is reduced by one order of magnitude, as will be evident from the numerical tests.

Let us now briefly comment on SD "with adjustable steps". Applying (2.15) to the wavefunctions gives :

$$\varphi_i^{(n+1)} = \varphi_i^{(n)} + \lambda_n F_i^{(n)}$$

$$F_i^{(n)} = -H\varphi_i^{(n)} + \sum_m \langle \varphi_m^{(n)}, H\varphi_i^{(n)}\rangle \varphi_m^{(n)} \qquad (2.1.26)$$

with λ_n minimizing the KS functional in the direction of forces $\{F_i\}$. In this case, however, the overlap matrix S reduces to

$$S_{ij}(\lambda) = \langle \varphi_j + \lambda F_j, \varphi_i + \lambda F_i \rangle = \langle \varphi_j, \varphi_i \rangle + \lambda^2 \langle F_j, F_i \rangle \tag{2.1.27}$$

since the orbitals are orthogonal to the forces. Indeed,

$$\begin{aligned} \langle \varphi_n(\mathbf{r}), F_l(\mathbf{r}) \rangle &= -\sum_j S_{lj}^{-1} \langle \varphi_n, H\varphi_j \rangle + \sum_{ijm} \langle \varphi_i, H\varphi_j \rangle S_{im}^{-1} S_{lj}^{-1} S_{mn} \\ &= -\sum_j S_{lj}^{-1} \langle \varphi_n, H\varphi_j \rangle + \sum_j S_{lj}^{-1} \langle \varphi_n, H\varphi_j \rangle = 0 \end{aligned}$$

Since this method has obvious drawbacks compared to CG and requires basically the same number of operations as CG we have done only a very limited number of tests with this method. In particular we tested the quadratic approximation to the inverse of the overlap matrix (2.1.27). Supposing orthonormality at the beginning of each step gives

$$S_{ij}^{-1\ (n+1)} = \delta_{ij} - \lambda_n^2 \langle F_j^{(n)}, F_i^{(n)} \rangle + O(\lambda_n^4)$$

Inserting this expression into the KS energy functional and minimizing it relative to λ_n gives

$$\lambda_n = -\frac{\sum_i \langle \varphi_i^{(n)}, H\varphi_i^{(n)} \rangle}{\sum_{ij} \left[\langle F_i^{(n)}, HF_j^{(n)} \rangle \delta_{ij} - \langle F_i^{(n)}, HF_j^{(n)} \rangle \langle F_i^{(n)}, F_j^{(n)} \rangle \right]}$$

This approximation turned out to be numerically unstable. This is probably due to the fact that λ_n may vary considerably and need not be a small quantity, as we empirically found.

We now discuss some more conventional diagonalization methods. The conventional diagonalization method has a slight advantage in providing automatically also the unoccupied KS eigenstates and eigenvalues. Since only occupied states appear in the KS energy functional, the minimization techniques provide us with occupied states only. It is often desirable to calculate the unoccupied states as well.

However, the minimization techniques provide us also with the self-consistent potential. Thus the unoccupied KS eigenstates and eigenvalues can be subsequently obtained, if required.

Also within the conventional self-consistent approach there are methods that avoid explicit diagonalization by exploiting the fact that typically only the lowest few roots are needed. One of those methods is the Davidson iterative method (DI) [15], which is widely used in particular by theoretical chemists. DI uses a first order correction for the N desired states $\{\psi_n\}$ as follows

$$\psi_n^{(1)} = \sum_{i=1}^{N} c_{in}(\psi_i^{(0)} + \Delta\psi_i^{(0)}) = \psi_n^{(0)} + \Delta\psi_n^{(0)}$$

$$\Delta\psi_i^{(0)} \approx \frac{(H - E_n^{(0)})}{E_n^{(0)} - H_{ii}}\psi_i^{(0)} \qquad (2.1.28)$$

The corrections $\{\Delta\psi_i^{(0)}\}$ are then included as basis vectors. $\{\psi_n^{(1)}\}$ are the lowest N roots resulting from diagonalization of a $2N \times 2N$ Hamiltonian matrix in the basis $\{\psi_i^{(0)}\}$, $\{\Delta\psi_i^{(0)}\}$. This iteration is repeated using progressively larger and larger matrices until the convergence is reached for a given H. Then the density (2.1.3) is updated and a new iteration cycle started until reaching the self-consistency. The number of operations is not directly comparable to that of preceding methods but scales as IN^2M.

In order to illustrate and compare how the methods introduced above work in practice, we present results for the ground-state electronic structure calculations of Si as follows *. A simple cubic supercell has been considered with eight atoms subject to periodic boundary conditions. The value $a = 10.26a.u.$, the experimentally observed lattice constant, was taken as the unit cell dimension. A first-principle non-local norm-conserving pseudopotential [16] was used to represent the electron-ion interaction. Exchange-correlation effects were described within the LDA approximation in parametrized form [17]. An energy cut-off of 7.0 Ry was

* The collaboration with S. Baroni on comparative DI calculations is gratefully acknowledged.

used, corresponding to 341 plane waves at the Γ point in the BZ. This model does not give a realistic description of the charge density. It is used here only for illustration purposes. Two types of structure have been tested. The first, in which the atoms were fixed in perfect diamond lattice positions will be referred to as ordered. In the other, referred to as disordered, the atoms were randomly displaced from their perfect lattice positions with maximum amplitude of 0.2 a.u. The initial conditions for the electronic orbitals were fixed by filling the lowest states resulting from diagonalization of a small 57×57 Hamiltonian matrix corresponding to an energy cut-off of 2.0 Ry.

The results are summarized in table 1.

*Structure**Method*	*SD*	*SD PJATV*	*DI*	*CG*	*Degree of freedom*
ordered	42	13	14 (4)†	11	*electrons*
disordered	251	222‡	34 (7)†	23	*electrons*

Tab.1. Comparison of several tested methods in No. of steps. Only the Γ point was used in BZ sampling. Convergence in seven significant figures is assumed. For SD $\frac{\Delta t^2}{M_i} = 0.16$ and 0.63 for the ordered structure in SD PJATV calculation. † - No. of self-consistency cycles. ‡ - This calculation was discontinued since the method became unstable when the convergence in the last significant figure was attempted.

It is evident that the CG method can reduce the number of steps I by roughly one order of magnitude with respect to SD (cf. the results for disordered structure). Concerning the PJATV algorithm, it is very efficient in the case of ordered structure. On the contrary for the disordered structure the time step fixed had to be equal to that of the SD method and the efficiency of PJATV algorithm becomes equivalent to the SD. Moreover in this case the PJATV algorithm suffers from the deficiency of being unstable when high precision is required . The instability appeared after the iterative step 222. The CG method compares very well also to DI. The number of steps is smaller. Although here the direct comparison of the CPU time is difficult, the results indicate saving up to one half of CPU time compared to DI.

To see the effect of a more careful BZ sampling on the CG minimization we have carried out a calculation where the BZ integral in the electronic density (2.1.3)

was approximated by summing over four special k points [13]. We considered the disordered system as introduced above. The energy cut-offs were chosen as in the previous calculation leading to 326 plane waves at the special k points and to 54 plane waves for the initial small matrix diagonalization. The results obtained using SD, DI, and CG methods are summarized in table 2.

$Structure \backslash ^{Method}$	SD	DI	CG	$Degree\ of\ freedom$
$disordered$	292	107 (6)†	64	$electrons$

Tab.2. Comparison of SD, DI, and CG methods in No. of steps. Four special k points were used in BZ sampling. Convergence in seven significant figures is assumed. For SD $\frac{\Delta t^2}{M_i} = 0.16$. † - No. of self-consistency cycles.

In the CG minimization with four special k points formula (2.1.24b) was used and a separate line minimization for each k point was carried out. The results are comparable to those obtained using the Γ point only.

We carried out another crucial test of the CG minimization by calculating the electronic structure of 2-d graphite. This system is known to be difficult to converge [18]. The hexagonal structure of graphite has been described by considering an orthorombic supercell with four atoms fixed in perfect lattice positions subject to periodic boundary conditions. The experimental unit cell dimensions with $a = 4.65 a.u., b = 8.05 a.u.$ have been used. The potential used was similar to that for Si [19]. We have carried out two calculations. One based on Γ point only, the other based on four special k points approximation to (2.1.3) [13]. An energy cut-off of 18 Ry was used, corresponding to 581 plane waves at the Γ point and roughly $\sim$ 240 plane waves for the four special k points. For both cases the initial conditions were fixed in a way similar to that of Si (The energy cut-off for the initial small matrix diagonalization was of 10 Ry).

The results are shown in table 3.

$Structure \backslash ^{Method}$	SD	CG	$Degree\ of\ freedom$
$2-d\ Graphite(1\ \mathrm{k}-point)$	289	40	$electrons$
$2-d\ Graphite(4\ \mathrm{k}-points)$	2764	104	$electrons$

Tab.3. Comparison of SD and CG methods in No. of steps. Convergence in seven significant figures is assumed. For SD $\frac{\Delta t^2}{M_i} = 0.083$.

The results confirm that the convergence of CG is very well also in this computationally complicated system.

2.2 TOTAL ENERGY (DOWNHILL) MINIMIZATION WITH RESPECT TO IONIC POSITIONS

We want now to explore the more complicated problem of minimizing the KS functional relative to the electronic and ionic degrees of freedom simultaneously. As discussed in section 2, this can be done very effectively by the dynamical simulated annealing strategy. However, one is often only interested in local minimization. In such a case it can be more effective to use alternative strategies. As for the electronic only case we discuss here the SD and CG methods.

The SD equation for ionic degrees of freedom reads

$$M_I \dot{\mathbf{R}}_I = \mathbf{F}_I = -\frac{\partial E}{\partial \mathbf{R}_I} = -\frac{\partial}{\partial \mathbf{R}_I}\left[\langle \Psi, H\Psi \rangle + E^{Irep}\right] \qquad (2.2.1)$$

where E^{Irep} is the energy of interionic Coulomb repulsion. In (2.2.1) the forces acting on ions have contributions from the electronic, as well as from the ionic subsystems. As in the section 2, the forces on the right-hand-side of (2.2.1) will have physical meaning only if the KS functional is close to its minimum value for that ionic configuration. In principle, it is possible to minimize the KS functional starting from arbitrary $\{\psi_i\}$ and $\{\mathbf{R}_I\}$. However, in nontrivial cases we found very difficult, if not impossible, to achieve convergence with a simultaneous electronic and ionic SD or CG minimization which started from an arbitrary $\{\psi_i\}$. It is more effective to minimize approximately the KS functional for a fixed initial $\{\mathbf{R}_I\}$, and then drive the system towards its local minimum by a combined electronic and ionic SD or CG minimization. In such a case the ions will be moved in the directions of forces that have to a good approximation their physical values.

We have tried to optimize the pure SD minimization by selecting appropriately the integration step and the electronic mass. The ionic mass was kept fixed. This is completely general since only the ratios $\frac{\Delta t^2}{M_i}$ and $\frac{\Delta t^2}{M_I}$ matter.

The results are in fig.2

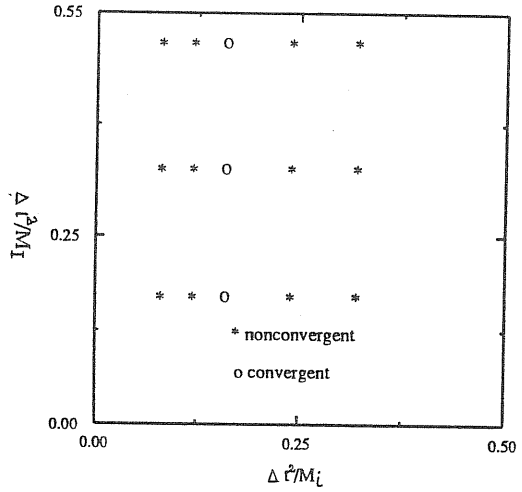

Fig.2. Convergence of the total energy SD minimization for different choices of parameters.

and indicate that the window of convergence within SD is extremely narrow for the electronic parameters. The points on the left-hand side of the convergent $\frac{\Delta t^2}{M_i}$ in the fig.2 did not converge because here the electronic optimization lagged behind the ionic motion, resulting in incorrect forces on ions. The non-convergence of the points on the right-hand side results from restrictions imposed by the largest G vectors (cf. the comments on PJATV method). Although small, there is a finite region of convergence. Within the narrow window of convergence no significant gain was found with the change of $\frac{\Delta t^2}{M_I}$. Generally, if one is only interested in minimization, the errors in the BO forces are not particularly severe and can be tolerated as long as they are smaller then the magnitudes of the forces. On the other hand the smallest errors in the BO forces are disastrous for the dynamics of the ionic subsystem as will be shown in the next section.

We have applied the CG algorithm (2.18) also to the ionic subsystem. The

main steps can be summarized as follows :

$$
\begin{aligned}
\mathbf{R}_I^{(n+1)} &= \mathbf{R}_I^{(n)} + \lambda_n \mathbf{h}_I^{(n)} \quad ; \quad n = 0, 1, 2 \cdots \\
\mathbf{h}_I^{(n)} &= \begin{cases} \mathbf{g}_I^{(n)} & \text{n=0} \\ \mathbf{g}_I^{(n)} + \gamma_{n-1} \mathbf{h}_I^{(n-1)} & \text{n=1,2,3}\cdots \end{cases} \\
\mathbf{g}_I^{(n)} &= \mathbf{F}_I^{(n)} = -\left[\langle \Psi, \frac{\partial H}{\partial \mathbf{R}_I} \Psi \rangle + \frac{\partial E^{Irep}}{\partial \mathbf{R}_I} \right] \quad ; \quad n = 0, 1, 2 \cdots \\
\gamma_{n-1} &= \frac{\sum_I \mathbf{g}_I^{(n)} \cdot \mathbf{g}_I^{(n)}}{\sum_I \mathbf{g}_I^{(n-1)} \cdot \mathbf{g}_I^{(n-1)}} \quad ; \quad n = 1, 2, 3 \cdots
\end{aligned}
\tag{2.2.2}
$$

λ_n must be chosen so as to minimize the following sum of energies along the direction h

$$E(\lambda_n) = E^{Ion} + E^{Irep} \tag{2.2.3}$$

This minimization procedure has been tested again for the disordered system. The results are shown in table 4.

*Structure**Method*	*SD*	*CG*	*Degree of freedom*
disordered	50	12	*initial electronic minimiz.*
	235	63	*electrons + ions*
	285	75	*total*

Tab.4. Comparison of SD and CG methods in No. of steps.

The two calculations have the same accuracy in the initial electronic minimization, as well as in the final electronic + ionic minimization. The energy was converged in six significant figures. Here the number of required iteration steps in the CG method is less favourable than in the purely electronic minimization. This may have two reasons. One may be that the use of a longer ionic displacement in the CG method can lead to non-physical ionic forces. The other reason may be inherent in the CG method itself, since it requires the Hessian matrix A to be SPD in the vicinity of each iteration point. Because of complicated topography of the energy surface this requirement is not valid generally, once the ions start to move. The method is expected to be more efficient close to the minima. An additional difficulty is the line minimization (2.2.3) which is a very time consuming procedure.

We have also tried to combine the SD minimization for ions with the more effective CG minimization for electrons, thus obtaining always the physically correct forces. We found that the combined ionic SD - electronic CG minimization results in a factor of $2 \div 3$ improvement compared to the case where the purely SD eqs. (2.9a,b) were used. This appears at present to be the most convenient approach although all the possible alternatives have not yet been fully explored.

2.3 DYNAMICAL SIMULATIONS OF THE IONIC SYSTEM

This section is devoted to the study of how the dynamical simulation of the ionic system is affected by the errors in BO forces introduced by different approaches to the electronic minimization. As already pointed out if the condition (2.8) is satisfied the interionic forces coincide with the physical BO forces.

There are essentially two strategies for doing the dynamical simulation of the ionic system using the BO forces on ions. One way, which will be referred to as adiabatic, consists of solving the eqs. (2.6a,b). Doing MD with the system defined by the Lagrangean (2.4) will keep the total energy of this dynamical system

$$E^{tot} = \sum_i \frac{1}{2} M_i \int d\mathbf{r} |\dot{\psi}_i|^2 + \sum_I \frac{1}{2} M_I \dot{\mathbf{R}}_I^2 + E\left[\{\psi_i\}, \{\mathbf{R}_I\}\right] \tag{2.3.1}$$

constant. In the instantaneous ground-state,when (2.8) is valid, the $\{\dot{\psi}_i\}$ are zero and effectively the total energy of the ionic subsystem

$$E^{Itot} = \sum_I \frac{1}{2} M_I \dot{\mathbf{R}}_I^2 + \Phi\left[\{\mathbf{R}_I\}\right] \tag{2.3.2}$$

si kept constant. Only when (2.3.2) is a constant-of-motion, the ionic dynamics will be correct. It means that the electronic configuration must have always enough time to relax to the instantaneous ground-state of the simultaneously changing ionic configuration. This poses a general question about whether the requirement of adiabaticity of the evolution of (2.4) is a realistic one. To set up such a regime requires $\{M_i\}$ to be small compared to $\{M_I\}$. Small $\{M_i\}$, in turn, require small time step Δt in the integration of eqs. (2.6). The accuracy of the BO forces can be checked by monitoring the constantness of (2.3.2).

The other conceivable way of calculation the BO forces for the ionic dynamics is based on complete decoupling of electronic and ionic dynamics by doing the minimization indicated in (2.8) explicitly. Having developed an efficient minimization technique to relax the electronic configuration gave us some hope to make this

approach, referred to as decoupled dynamics, more efficient than the adiabatic one. In particular, the decoupled dynamics should relax the requirement of keeping the time step in the integration of the equations

$$M_I \ddot{\mathbf{R}}_I = -\frac{\partial \Phi}{\partial \mathbf{R}_I} \tag{2.3.3}$$

small.

To test how the two above mentioned methods work in practice we have excited a phonon mode in the system consisting of eight Si atoms in diamond lattice sites. The atoms were initially displaced from their equilibrium lattice positions in the direction of the eigenmode $\epsilon_{\Gamma_{25'}}$, corresponding to the optical phonon mode at the Γ point of the supercell BZ. This was the only point considered in the BZ sampling leading to a rather poor representation of the electronic density n(r). The same potential as before was used. The system with displaced ions was initially prepared in ground-state, then the ions were left to move under the action of the BO forces.

The results obtained using the adiabatic dynamics are shown in fig.3. The atoms perform oscillations with frequency $f \approx 18THz$. This fairly good result confirms that the thickness of the BO surface, though finite, was adequate. We performed also a series of calculations following the strategy of decoupled dynamics. The time step Δt has been fixed to $3 \div 4$ times larger than that used in the adiabatic dynamics. The CG minimization technique for the electronic degrees of freedom was used. The result is shown in fig.4. The phonon is damped what means that the forces on ions were not calculated correctly. It must be stressed that this feature is present also using other minimization procedures, like SD.

Generally, this might have two reasons. Either the time step used was too large or the system was not brought properly into its instantaneous ground-state. By discretizing numerically the one-dimensional oscillator equation

$$M_I \ddot{R}_I = -\omega_0^2 R \tag{2.3.4}$$

with ω_0 - being the optical phonon frequency, using the Verlet algorithm[10] we checked that the time step used was adequate. To see how the precision of elec-

tronic minimization influences the results we performed a series of calculations fixing different precisions for the electronic minimization procedure. These results are depicted in figs. $5 \div 8$. It is evident that unless the precision of electronic minimization is very high the forces are badly calculated. Even the convergence in ten significant figures, requiring roughly ten electronic CG steps for each ionic step, was not sufficient. The necessity of very high precision in the electronic minimization makes the adiabatic dynamics much more efficient and superior to the decoupled dynamics.

This rather surprising behavior has the origin in a cancellation of errors produced by MD that is missing in the other approach [20],[21]. The MD equation-of-motion for the electronic wavefunctions is

$$M_i \ddot{\psi}_i = F_i \tag{2.3.5}$$

stating the proportionality of the acceleration of the wavefunction to the force acting on it. In the ground state the wavefunctions do not move, the forces are zero. When the ions displace the forces on the wavefunctions become non-zero and proportional to the ionic displacement. Thus the electronic wavefunctions will accelerate and catch up the delay until overtaking the ions when the forces begin to brake the motion of the wavefunctions. The electronic oscillations make the ionic forces to oscillate, causing the cancellation of errors. In other words the electronic and ionic dynamics are correlated .

On the other hand in the decoupled dynamics the electronic wavefunctions obey first order equations of the SD type

$$M_i \dot{\psi}_i = F_i \tag{2.3.6}$$

making the velocity of the wavefunctions proportional to the forces on orbitals, leading to a systematic delay and error in the BO forces.

To bring the above reasoning on a firmer ground we have studied a simple model consisting of two coupled (anharmonic) oscillators simulating the motion of a heavy

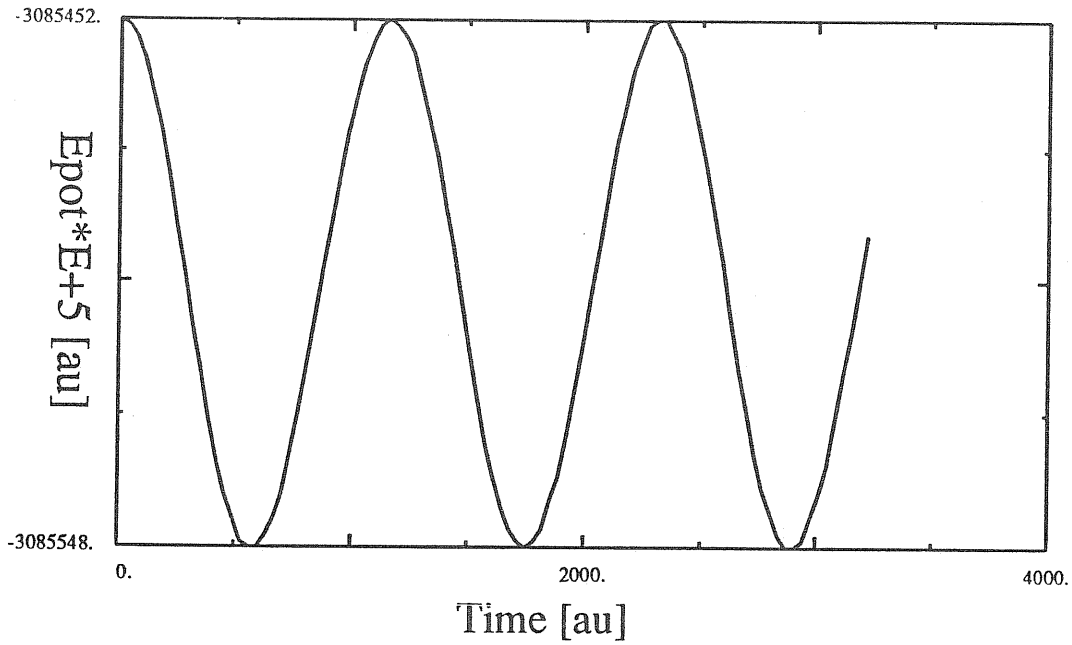

Fig.3. The evolution of the potential energy in the "adiabatic regime"; Δt and M_i were taken to be 7.0 and 300. a.u., respectively.

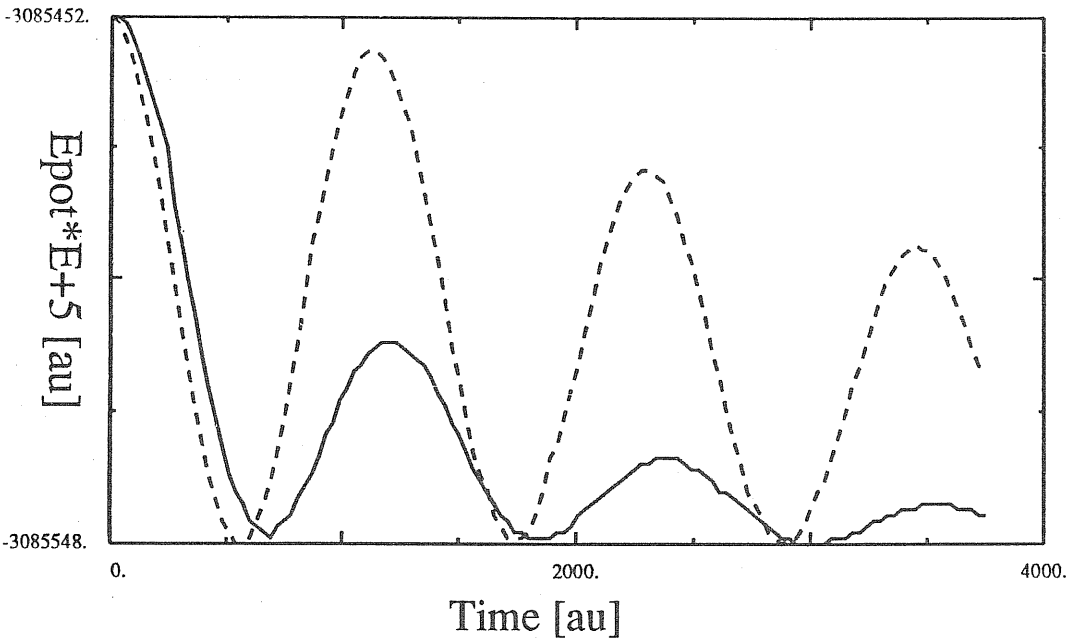

Fig.4. The evolution of the potential energy in the "decoupled regime"; Δt was taken to be 30. a.u. Full line: one electronic CG step for each ionic step; dashed line: two electronic CG steps for each ionic step.

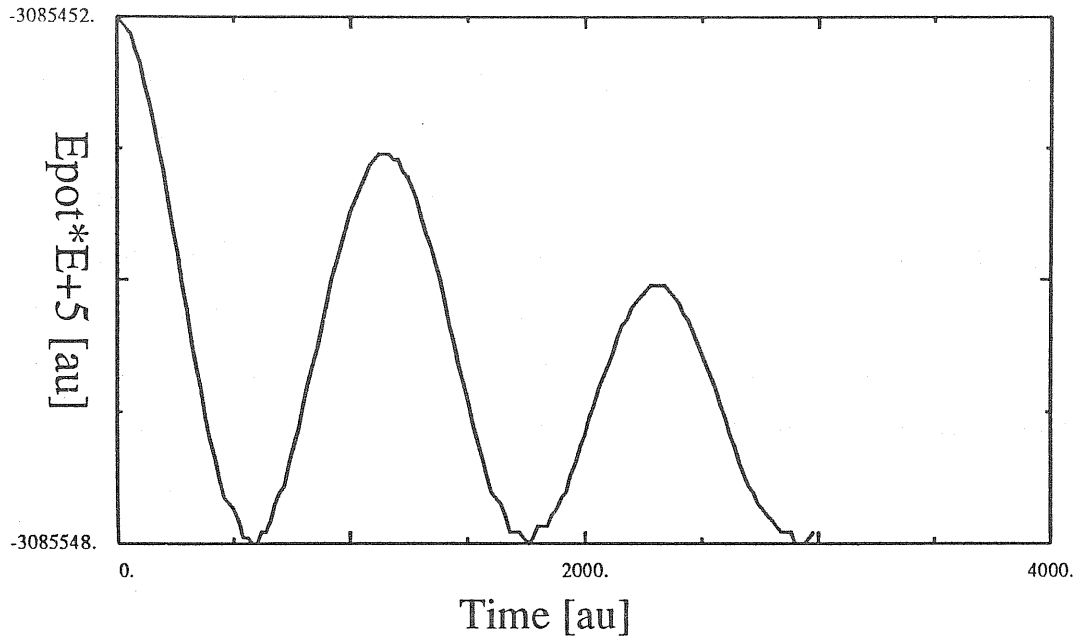

Fig.5. The evolution of the potential energy in the "decoupled regime"; Δt was taken to be 20. a.u. The electronic CG minimization for each ionic step was converged in seven significant figures.

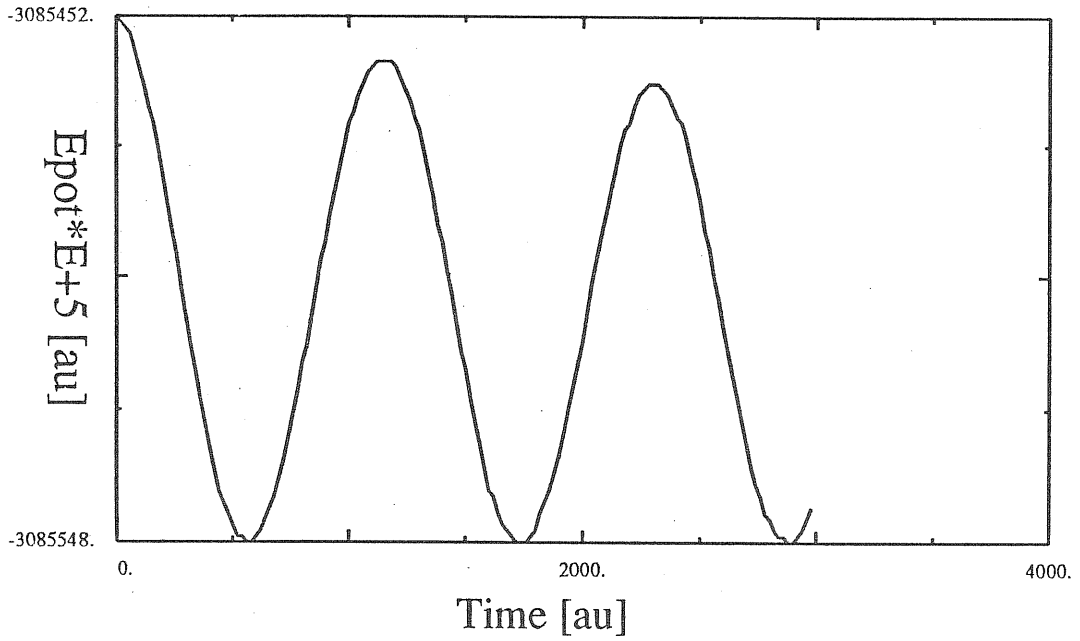

Fig.6. The evolution of the potential energy in the "decoupled regime"; Δt was taken to be 20. a.u. The electronic CG minimization for each ionic step was converged in eight significant figures.

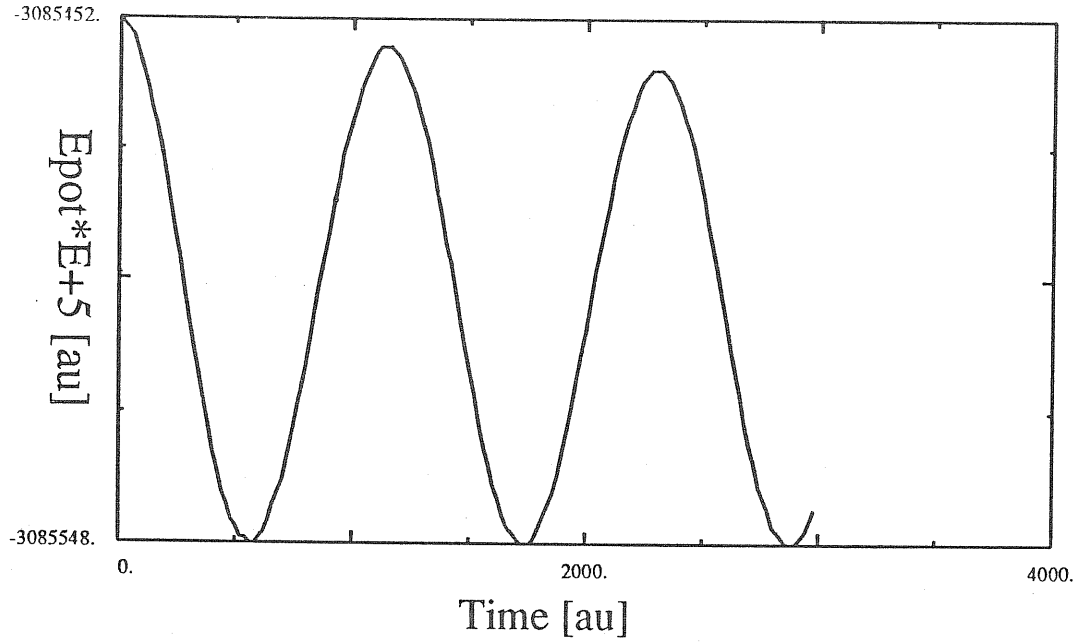

Fig.7. The evolution of the potential energy in the "decoupled regime"; Δt was taken to be 20. a.u. The electronic CG minimization for each ionic step was converged in nine significant figures.

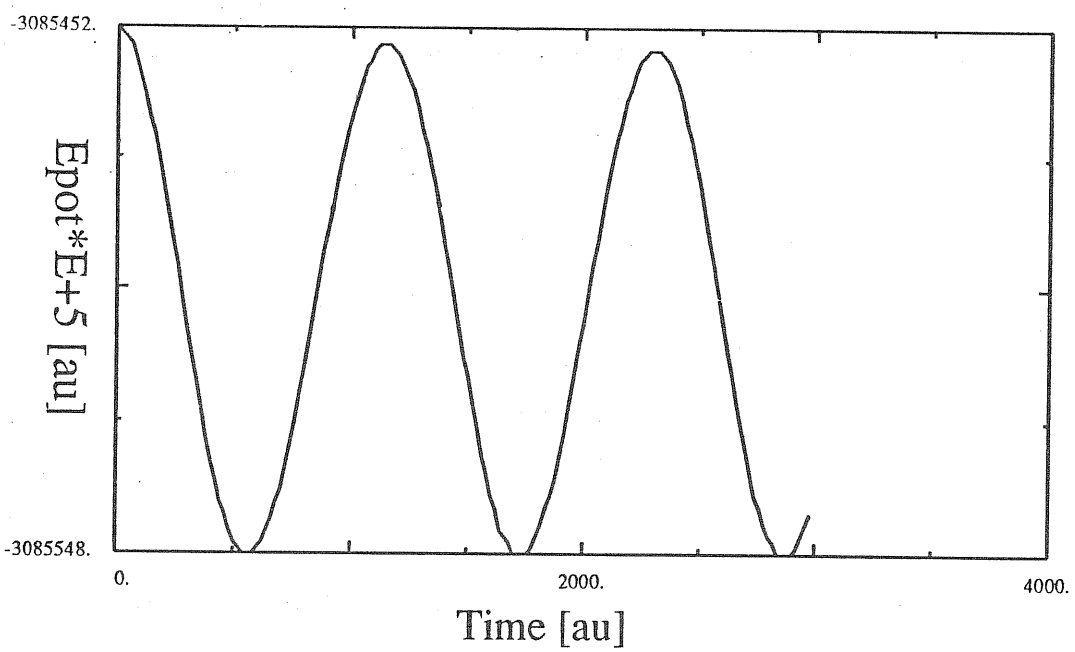

Fig.8. The evolution of the potential energy in the "decoupled regime"; Δt was taken to be 20. a.u. The electronic CG minimization for each ionic step was converged in ten significant figures.

particle (ion) coupled to a light particle (electron). The model has been studied in both adiabatic and decoupled dynamics. In the adiabatic dynamics we found slight oscillations of the total energy of the ionic subsystem, introducing, however, no systematic shift in the constant-of-motion. The heavy particle oscillates slightly around the exact position, causing the cancellation of errors in the forces. In the decoupled dynamics there was a systematic shift in the energy of the heavy particle and correspondingly a systematic error in the forces. A work on a more realistic model is underway.

Chapter 3

AMORPHOUS AND LIQUID STATES FROM TOPOLOGICAL VIEWPOINT AN APPLICATION TO AMORPHOUS AND LIQUID SILICON

In order to fix ideas for the following two sections we give in this part a review of amorphous (a) and liquid (l) states based on a topological approach. The structural constituents, the structure and symmetry, as well as the influence of the constituents on the universal and specific properties of these systems are briefly discussed [22]. Particular attention is paid to the topological properties of a- and l- silicon.

Topology is particularly important in presence of *structural disorder*, found in liquids and amorphous metals and in the case of *topological disorder*, found in amorphous semiconductors. In the latter case the long-range-order is naturally absent, whereas the short-range-order is maintained to a considerable extent. The structure can be described by a *regular graph.*

In covalent systems, the vertices and the edges of the graph are atoms and bonds, respectively and faces are rings. The atoms have fixed chemical valency, so that the graph has a fixed vertex coordination z (z=4 for Si), and is said to be *regular.* This graph is called a *continuous random network* (CRN). However, in real systems there are also *coordination defects* violating the regularity of the graph. These defects will be briefly discussed for a-Si.

In metallic systems, where the effects of covalency are absent, only vertices (atoms) have a direct physical meaning, the edges are defined by "Voronoi tessela-tion", the analogue of Wigner-Seitz cells or Brillouin zones encountered in crystals. This new graph called *Voronoi froth* is related to the original packing by duality and is regular.

Voronoi froths and CRNs are locally topologically equivalent having the same

low vertex coordination z=4. What distinguishes them topologically is the ring statistics. In fact, amorphous materials, but also aggregates of metallurgical grains, foams, soap bubble froths or photographic emulsions, etc... are all *random cellular structures*. Although we will concentrate only on CRNs, there seems be a kind of universality in all random cellular structures [22]. All of them have identical main structural features.

The most immediately striking feature of CRNs which distinguishes them from crystalline networks is the presence of rings containing an odd number of bonds (odd-membered rings) *. Indeed, only rotations by $2\pi/n, n = 2,3,4,6$ are compatible with translational symmetry. The odd-membered ring can be imagined as produced by a Volterra procedure by cutting through to the centre of a six-fold ring, removing or adding a wedge-shaped piece and regluing. Thus the odd ring can be thought of as surrounding the core of a disclination.

Odd rings are not found in isolation. In three dimensions they are threaded through by continuous lines (disclination-, odd- or Rivier-lines) [25] which form closed loops or terminate on the surface of the material. The geometric argument relies on an observation about the allowed configuration of edges e and the number of i-sided faces f_i on a closed surface S. The incidence relation between edges and faces, $2e = \sum i f_i$ implies that $\sum_{i\ odd} i f_i = even$, and because if_i and f_i have the same parity for i odd

$$\sum_{i\ odd} f_i = even \qquad \forall S \tag{3.1}$$

i.e. also on the surface of a fundamental polyhedron of rings. This guarantees the occurrence of odd rings by pairs. Eq. (3.1) can be regarded as the first topological conservation law.

* There are also some models of random structures free of odd-membered rings, called trivial (or flat). Examples of such models are Connell-Temkin model of CRN [23] or Mattis model of spin glass [24].

The second conservation law is the Euler's relation

$$-c + f - e + v = 0 \tag{3.2}$$

for a three dimensional graph with c cells, f faces, e edges, and v vertices.

The purely topological arguments also confirm that odd lines are structurally stable universal constituents of random structures. The topological classification scheme of possible structural defects used for ordered systems[26] and for more general systems[27] can be extended also to random systems [25],[28]. The chief conclusion of this analysis is that in three dimensions there is a one-to-one correspondence between the group Z_2 -the group isomorphic to the integers modulo 2- and the physical states of the amorphous solid. Rivier argues [25] that there is a stable line defect, which is a disclination whose intensity can be identified with the oddness of the rings along the disclination line - both are defined modulo 2.

The Z_2 group can be related to two possible transformations when a closed path is described : a rotation by 4π is homotopic to identity, whereas a 2π rotation is not. This can easily be visualized by considering for simplicity the case of a spin glass with antiferromagnetic interactions on a topologically disordered lattice which contains odd rings. An odd ring cannot accommodate a configuration of spins minimizing the energy of all its bonds, see fig.1.

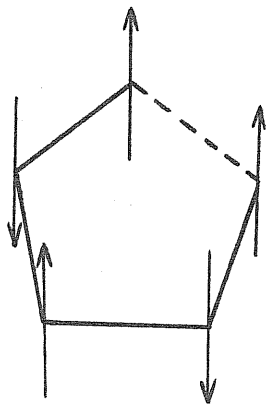

Fig.1. Frustrated odd ring containing antiferromagnetic interactions.

It is frustrated, the frustration being characterized by the group Z_2.

The 2π-disclination is also the only structural constituent surviving the transi-

tion from network to continuum [22]. The transition can be thought of as the result of succesive decoration of the original network, adding new vertices and edges until the "continuum limit" is reached. It is easy to visualize the decoration in two dimensions, where it consists of replacing each vertex of the network by a hexagon (fig.2).

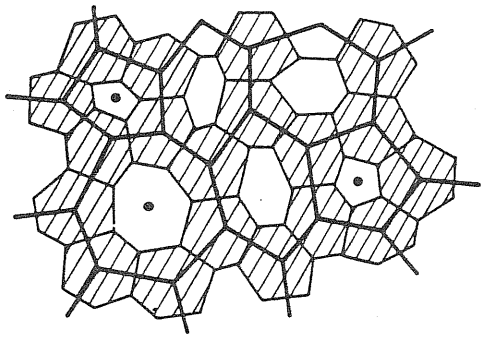

Fig.2. Decoration in two dimensions.

The odd rings are invariant, puncturing the random space. In three dimensions each vertex is replaced by a truncated octahedron. These octahedra are joined by four of their hexagonal faces, allowing for two limit configurations- *staggered* and *eclipsed* and an infinite number of intermediate configurations in the CRN (fig.3).

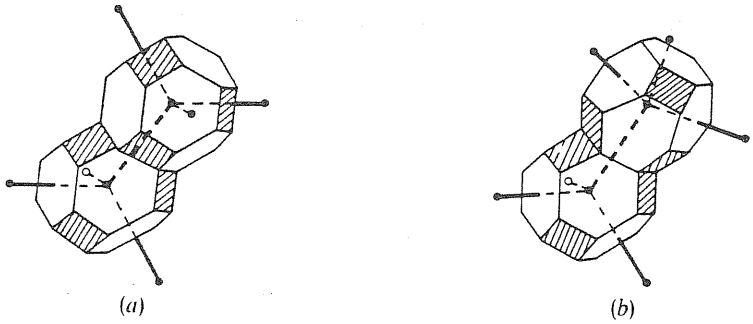

Fig.3. Staggered (a) and eclipsed (b) configurations in CRN and in decorated structure.

The mutual angle between tetrapods characterizing the configuration is called the *dihedral angle*. The existence of dihedral angles which are neither of the eclipsed,

nor the staggered type is symptomatic for frustrated systems characterized by the group Z_2.

Let us now very briefly come to the way in which the structural constituents (odd lines) are believed to influence the universal properties of amorphous materials. Most of them have a natural topological formulation.

The odd lines are suspected to cause the low energy *tunneling modes* in glasses. These modes cause anomalous low temperature properties ($\simeq 1K$) [30]. It can be shown theoretically, based on symmetry arguments only, that there are two classical ground-state configurations per odd line [31],[32] referred to as $|0\rangle$ and $|2\pi\rangle$. They are related by a gauge transformation, a 2π-rotation, and the system can tunnel between them (this reflects the Z_2 structure of the odd line).

Similar topological analysis, based on calculation of entropy and energy of odd lines [29], gives also some explanation of properties of amorphous systems at high temperature. It leads to a formula that is identical to what is known as the empirical Vogel-Fulcher law, thus yielding some argument that amorphous and liquid states have the same kind of topological defects, but very different physical properties. At high temperatures odd lines expand and shrink, while remaining uninterrupted. They become frozen punctures at low temperature.

The odd lines are suspected to influence also the electronic structure of CRNs. The main conclusion of the topological analysis of the electronic energy spectrum (EDOS) is that a completely anti-bonding state is not realizable in a structure containing odd rings. This causes the EDOS to be strongly suppressed near the anti-bonding edge. Thus states near this edge are expected to be affected by the topological disorder, in particular by the ring statistics. The schematic EDOS of a topologically disordered system containing odd rings and no long-range-order is shown in fig.4.

Here a simple tight-binding Weaire-Thorpe Hamiltonian has been assumed [33],[35].

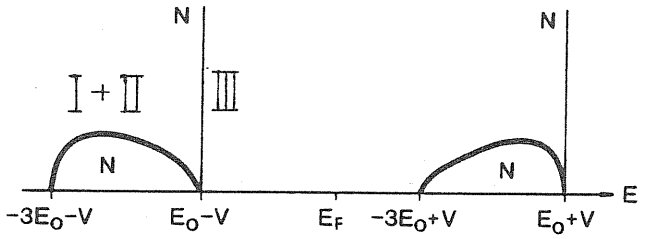

Fig.4. Schematic electronic energy spectrum (EDOS) of a-Si. E_0 is the on site and V is the intersite tight-binding parameter of the Weaire-Thorpe Hamiltonian.

The spectrum is skew near the band gap edges. This occurs because anti-bonding wavefunctions cannot be accommodated in regions containing odd rings. Another feature is related to the absence of long-range-order in amorphous systems. If, for example, we considered a crystalline Hamiltonian, there would be two peaks (Van Hove singularities) in its spectrum (called I,II) and a delta function (called III). If no long-range order is present, peaks I and II merge into one broad peak (I+II), as illustrated in fig.4. This behaviour was observed also experimentally [36].

Topological analysis can account also for other anomalous properties, like vibration modes, elastic energy or the Hall effect [22].

Real systems, however, can always contain also some coordination defects. Until recently only undercoordination defects have been considered. Calculations show that overcoordination defects may have comparable energies [37]. We shall consider here three-fold T_3 and five-fold T_5 coordinated atoms. It is elementary to show within simple models (like the Weaire-Thorpe) that these defects introduce states lying in the gap .

3.1 TOPOLOGICAL PROPERTIES OF a-Si

In this chapter we discuss the topological properties of models of a-Si as generated by an ab-initio MD [38],[39]. The method used is that described in section 2. Basically, a constant volume MD simulation with an FCC unit cell containing 54 atoms periodically repeated was carried out. The simulation was started from l-Si. The amorphous structure was prepared by a very rapid quenching from the melt to a final temperature of $300K$.

In section 3 the role of odd rings and lines was pointed out. Since the odd rings are not a priori required in generating a CRN and their effects on the radial distribution function are rather subtle, the only experimental evidence for the existence of odd-membered rings may come from observed differencies between the XPS spectra of c- and a-Si (merging of peaks I and II [36]). However, this possibility has recently been questioned [40] on the basis of experimental uncertainty. Moreover, recent high-resolution transmission electron microscopy experiments on a-Si gave some support to a submicrocrystalline model [41]. Thus the question of a realistic model for a-Si and the role of topology remains open. Reliable theoretical calculation, such as that of refs. [38],[39] and its subsequent analysis [46] might help to answer some of these questions.

The model analyzed here differs from many other existing models [23],[42] in being an ab-initio model conformed to periodic boundary conditions. Periodic boundary conditions enable surface effects to be avoided and long-range interactions to be included in an easy way. No arbitrary assumption is made on the interaction potential which is obtained as discussed in section 2 from accurate LDA calculation. The most obvious disadvantage of the present model is the effect of small size of the unit cell.

The radial distribution function for the generated model is presented in fig.5.

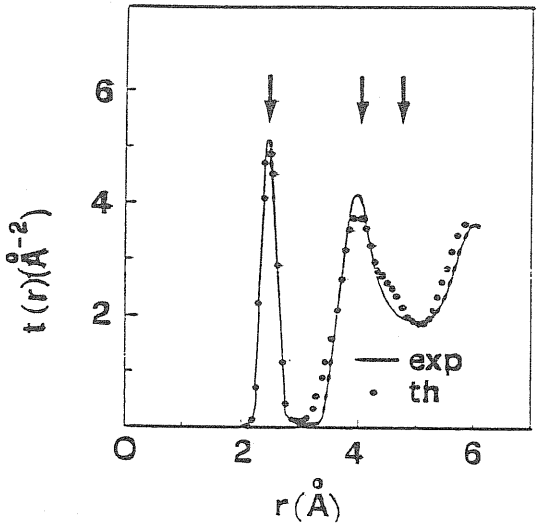

Fig.5. Radial distribution function for a-Si [39]

The integral over the first peak gives a local coordination of four. The *geometric distortion* is usually quantitatively measured by the rms bond-angle deviation. Our model has a rms deviation of $\approx 14°$, a value slightly larger then the commonly accepted value $\approx 10°$.

However, it is equally, or even more important, to have a measure of the *topological distortion.* This can be measured by *ring statistics.* Useful information could provide also the odd-lines (cf. 3). Their study is prevented here by a small size of the unit cell.

We have written a program enabling a complex structural and topological analysis of our models, including bond-, and dihedral angle analysis as well as ring statistics. Our definition of the dihedral angle is that of ref. [43], and the definition of the ring statistics is based on a shortest paths analysis as suggested in refs. [44],[45]. The shortest path analysis takes, in turn, each atom in the structure as a starting point and connects each couple of bonds attached to it through the structure in the shortest possible path. This definition of ring statistics has the advantage of yielding a distribution for n-fold rings which is zero at high n.

The results of ring statistics analysis [46] are in tab.1 and in fig.6

n:	3	4	5	6	7	8	9
$R_c = 2.7\mathring{A}$	0.111	0.222	2.128	2.382	0.728	0.317	0.061

Tab 1. Ring statistics for a-Si

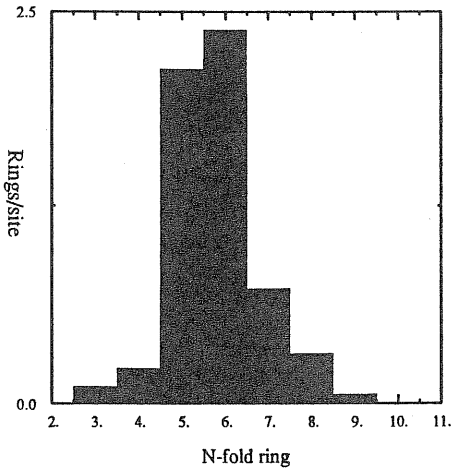

Fig.6. Ring statistics for a-Si

The neighbour was defined by a cut-off taken from the pair correlation function as $R_c = 2.7\mathring{A}$. The result is an average over 16 configurations generated by MD. At this R_c there were two T_3 atoms. One of them annihilated continuously, creating a T_5 atom and vice-versa. This process triggered a small change in the ring statistics affecting mainly the number of five-fold rings. The analysis has revealed a large portion of odd rings dominated by five-fold rings. Furthermore we found that seven-fold rings are rarely attached to five-fold rings. This renders the so-called hair-pin configuration of disclinations, proposed as a mechanism of screening the stress due to disclinations [29], as rather improbable. In our model only two atoms are not members of any odd ring and no atom lies in a local diamond-structure environment. Thus this model is a member of the purely amorphous class of structures.

Any frustration due to odd rings is accompanied by a broad distribution of the dihedral angles (only staggered configuration-60°, and eclipsed configuration-0° are permitted in crystals).

The dihedral angle distribution for our model (again averaged over 16 configurations) is in fig.7

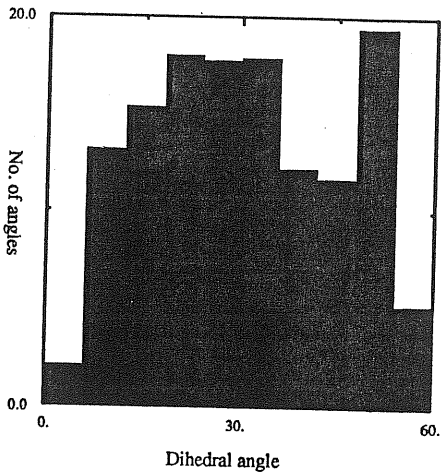

Fig.7. Dihedral angle distribution for a-Si

The unusual feature of our model is the decrease in the distribution about the staggered configuration, indicating once more no residual diamond-like order present. In the other existing models [42] the staggered configuration is usually much more frequent than the eclipsed one. This may be the effect of small unit cell size in our model, since the dihedral angle calculation involves the third neighbours. The important point, however, is that the staggered configuration in crystals gives rise to a third-neighbour peak at 4.7$\mathring{A}$ which is absent in the experimental pair-correlation function [45]. Moreover, the relative frequency of appearance of the eclipsed and staggered configurations is associated with five-fold rings [23], which are clearly dominating in our model. Thus it is not clear whether the unusual shape of the dihedral angle distribution is to be regarded as a deficiency.

It is tempting to try to analyze the electronic density-of-states EDOS from the viewpoint of topology (cf. section 3).

The EDOS for our model is in fig.8.

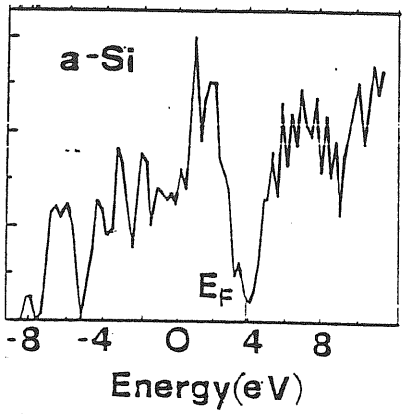

Fig.8. Electronic density-of-states for a-Si [39]

Here the results are rather inconclusive. Though there are three well separated peaks in the valence band, the separation of peaks I and II might occur as an effect of small unit cell size, rather than for topological reasons. As a consequence of coordination defects, there are gap states near E_F.

3.2 TOPOLOGICAL PROPERTIES OF l-Si

This part deals with topological properties of l-Si, generated again by the ab-initio MD. The model, as before, consists of 54 atoms enclosed in an FCC unit cell conformed to periodic boundary conditions [38].

In section 3 we have given arguments that the symmetry of high- and low- temperature phases should be the same. The topological analysis of l-Si is interesting also because, unlike for a-Si, there are very few realistic models of l-Si. As far as we know the best model generated so far uses the empirical Stillinger-Weber (SW) potential [47],[48]. Though l-Si is operationally an important phase, very little has been done both experimentally and theoretically.

The radial distribution function for our model is in fig.9.

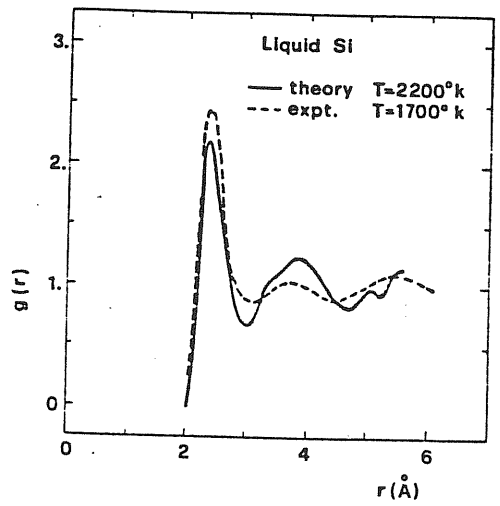

Fig.9. Radial distribution function for l-Si [38]

The average number of neighbours obtained by integrating over the first peak of g(r) is 5.4, i.e. less than 6.4 obtained from experiment. The agreement with the experiment is less satisfactory than for a-Si. Likely here the effect of small unit cell is more pronounced.

The results of ring statistics analysis [46] are in tab.2. and fig.10.

n :	3	4	5	6	7	8	9	10
$R_c = 3.04\mathring{A}$	1.711	1.920	3.359	2.550	0.746	0.043	0.002	—
n :	3	4	5	6	7	8	9	10
$R_c = 2.65\mathring{A}$	0.195	0.201	0.797	0.891	0.744	0.603	0.439	0.422
n :	3	4	5	6	7	8	9	10
$R_c = 2.49\mathring{A}$	0.021	0.037	0.319	0.254	0.171	0.191	0.186	1.285

Tab.2. Ring statistics for l-Si for different values of R_c

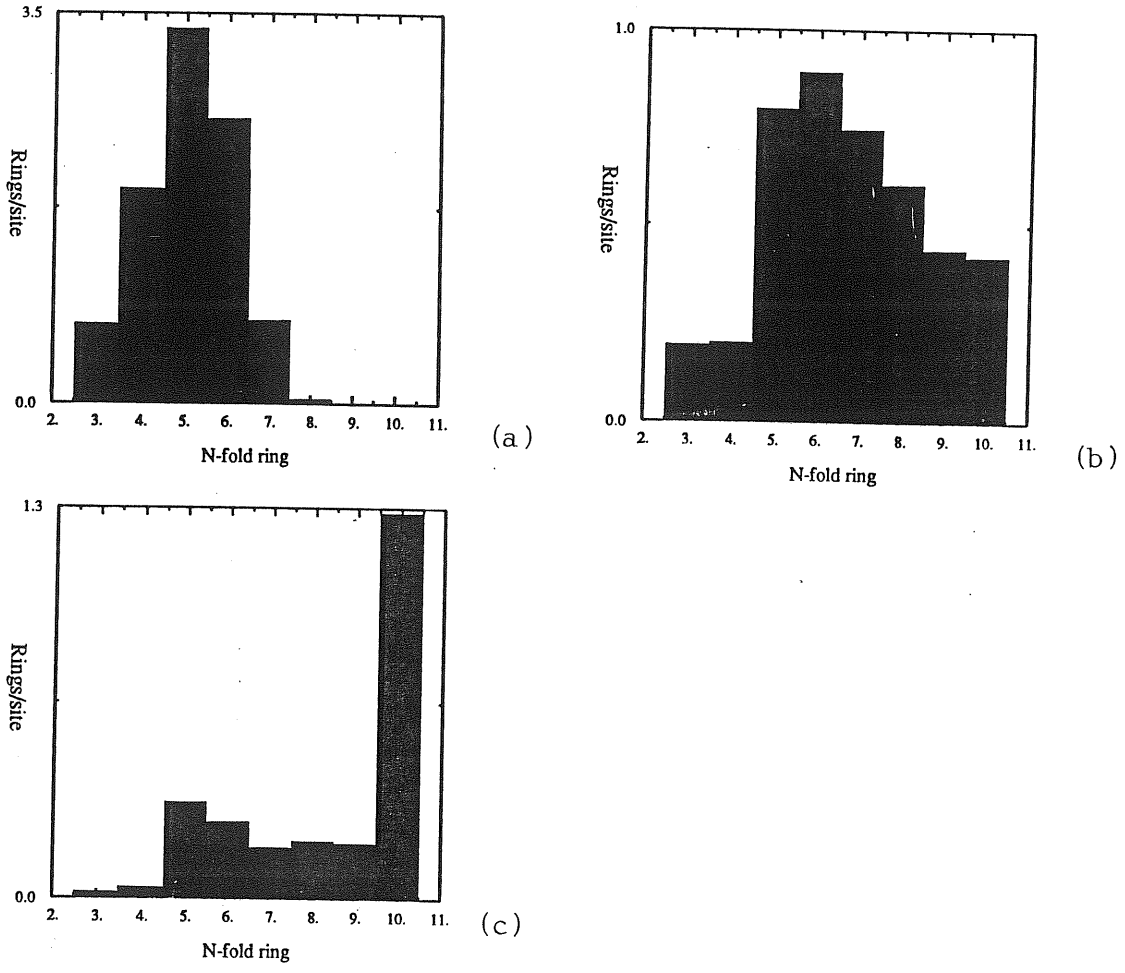

Fig.10. Ring statistics for l-Si for different values of R_c. In a) $R_c = 3.04\mathring{A}$, b) $R_c = 2.65\mathring{A}$, and c) $R_c = 2.49\mathring{A}$.

Here we were faced an additional problem, namely the definition of neighbour. The analysis has been carried out with three values of R_c: $3.4, 2.65, 2.49\mathring{A}$. The

results are averages over 10 configurations generated by MD. The result obtained with the largest value of R_c corresponds to the first minimum of g(r), while the value $R_c = 2.65$ is close to the value found in c-Si and to the value taken from the inherent structure calculation, as will be shown in following. Compared to a-Si the distribution is much broader especially on the high n side. The ratio of 6 : 7 fold rings changes significantly from l- to a-Si.

The EDOS of our l-Si is in fig.11.

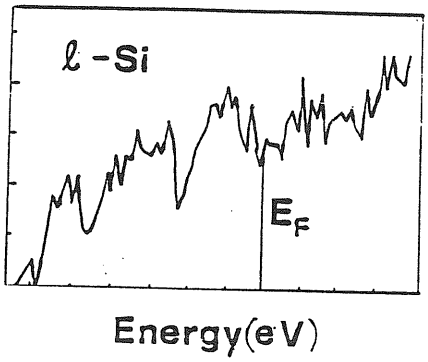

Fig.11. Electronic density of states for l-Si [38],[39]

The behaviour is very much free-electron like, yielding a metal, as it should, but as before, the topological analysis (cf. 3.) for our small model is rather inconclusive.

It is interesting to attempt a separation of packing and vibration effects for a liquid [47],[49],[50]. The idea is based on partitioning of the multidimensional potential energy surface Φ for an N-atom system. The purpose is to assign any configuration of atoms uniquely to one local minimum. The displacement of the configuration from a minimum is simply regarded as a "vibrational" displacement. This separation is based on the following exact expression for the Helmholtz free energy [49]

$$F = F_0(T) + N \min\{\Phi + f_v(\phi, T) - k_B T \sigma(\phi)\} \qquad (3.2.1)$$

where F_0 is an additive part of F (irrelevant here), σ is the logarithm of the density of potential energy minima, and f_v is the mean vibrational free energy for those regions whose minima lie at $\Phi = N\phi$. The principal result is that the *inherent struc-*

ture of a liquid obtained after removing the "vibrational" displacement is virtually temperature-independent.

There is a simple procedure for partitioning the Φ surface; Any configuration is assigned to the minimum that is encountered when moving downhill from the starting point into the local minimum (except for a zero measure manifold).

Although the atom arrangements which contribute to the inherent structure are amorphous, the real a-Si will indoubtedly differ in properties depending on method of preparation.

To sample the minima of the Φ surface by a sequence of downhill minimizations starting from configurations generated by MD for a liquid is a very demanding task when using an ab-initio technique outlined in section 2. For this reason and because the liquid is less satisfactorily described by the small model we have carried out only a single minimization. The minimization was started by a purely SD minimization, followed by combined electronic CG- ionic SD minimization and finally, very close to the minimum, an electronic + ionic CG minimization was used. The corresponding pair correlation function as well as that for the starting configuration are in fig.12

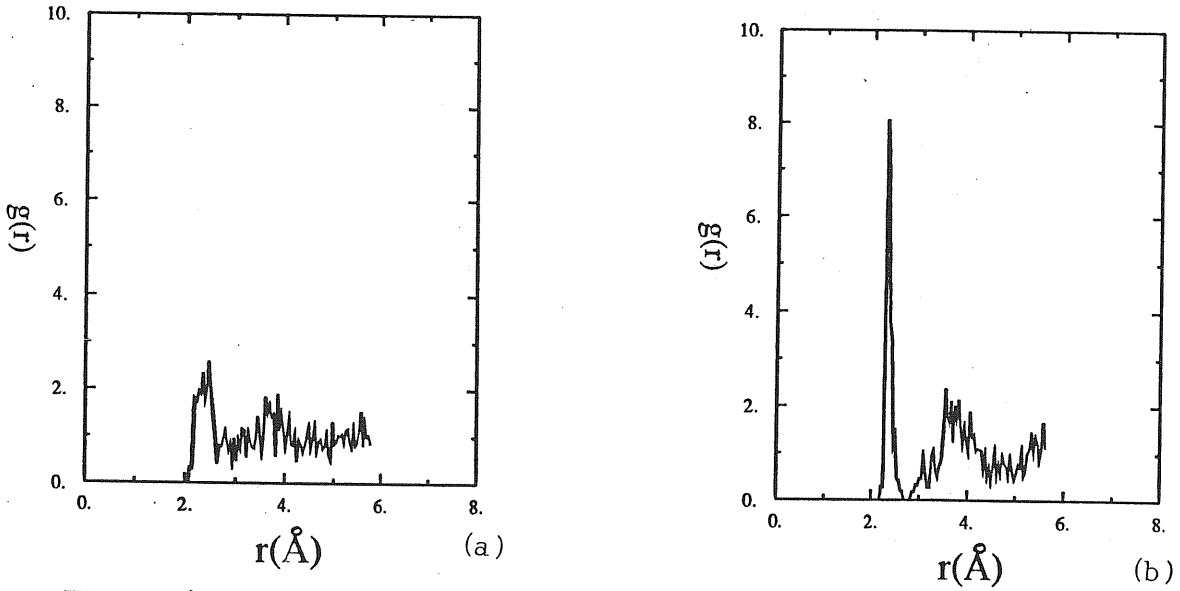

Fig12. a) Radial distribution function for the initial configuration. b) Radial distribution function after mapping onto the nearby minimum.

This result is a very preliminary one. The g(r) resembles the main features of the inherent g(r) for l-Si as obtained using the SW potential and averaging over several configurations [47]. The main difference is a less pronounced second peak and an entirely separated first peak (fig.13.).

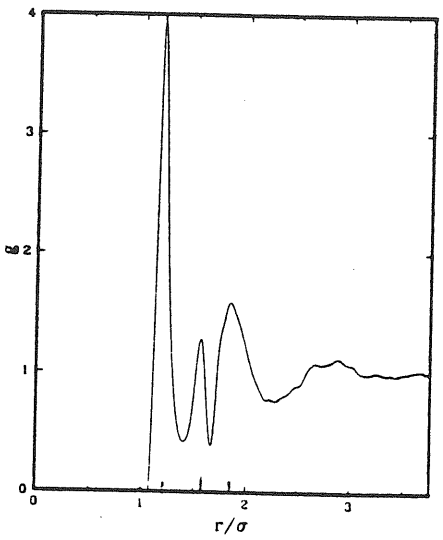

Fig13. Radial distribution function for the inherent structure of l-Si calculated using the SW potential [47]. $\sigma = 2.095\mathring{A}$.

The well separated first peak dies out at $R_c = 2.73\mathring{A}$ in our calculation. This suggests the use of this distance as the cut-off criterion for examination of ring statistics for l-Si, although alternative definitions are possible. The integral over the first peak gives a running coordination number very close to four. The number of coordination defects is larger than in a-Si. We found four T_3 atoms and one T_5 atom.

As anticipated before the properties of this system may be very different from a real a-Si. In particular, we have carried out the ring statistics analysis for this system with $R_c = 2.73\mathring{A}$. The result is in tab.3 and fig.14 and yields topological properties very different from those of a-Si.

n :	3	4	5	6	7	8	9	10
$R_c = 2.73\mathring{A}$	–	0.148	2.481	1.352	1.500	0.259	0.056	–

Tab.3. Ring statistics as obtained after mapping the system onto the nearby minimum

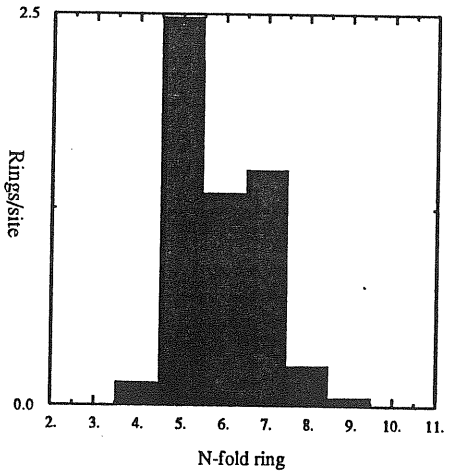

Fig.14. Ring statistics as obtained after mapping the system onto the nearby minimum

The predominance of odd rings can, of course, be averaged out in a more careful Φ-surface sampling, but there is some indication that this will not be the case.

We have calculated also EDOS for this system with result depicted in fig.15

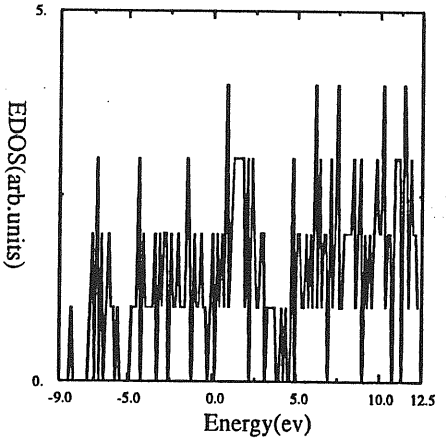

Fig.15. Electronic density of states as obtained after mapping the system onto the nearby minimum

This EDOS resembles the main features of that of a-Si. Again, as before, the resolution is insufficient to judge the influence of the ring statistics on the electronic properties.

Chaper 4
CONCLUSIONS

From our work we can draw the following conclusions:

There are several possible ways of minimizing the energy functional (2.2), depending on the problem at hand. We have developed a new efficient and robust method for solving the standard electronic structure problem for fixed ionic positions based on the conjugate gradient strategy. The performance of the method was tested on several systems and compared with other methods, in particular with the steepest descent, the Payne, Joannopoulos, Allan, Tetter, Vanderbilt method and with the Davidson method. In all these cases our method was found better than or at least comparable to all the other methods. The rate of convergence is not strongly system-dependent. The method is general and works also in cases when some of the other methods fail. We expect that this method, that falls into the class of non-diagonalization methods, will allow to treat still larger and more realistic systems that are now at or behind the present computational limits. The conjugate gradient strategy was applied also to the minimization of the energy functional (2.2) with respect to ionic positions. However, here the situation is more complex and the results less favourable. Last but not least, we have demonstrated that only the so-called adiabatic dynamics is feasible in ab-initio dynamical simulations of the ionic system. The reason of this behaviour was traced to the cancellation of errors produced by molecular dynamics, that doesn't arise when the second-order differential equations for the electronic orbitals is replaced by a first-order equations of the steepest descent type.

In the other part we have carried out analysis of models of amorphous and liquid silicon generated by methods described in the first part. A first step has been done towards understanding the inherent structure of liquid silicon. Particular attention was paid to the topological properties of these systems. They have been

found topologically non-trivial, containing a large portion of odd rings. There is some indication that the inherent structure of liquid silicon might be topologically very interesting. The odd rings are expected to account for the unusual properties of these systems. The study of our small model doesn't allow to make any definite conclusion about the correlation between the physical properties and the presence of a large number of odd rings. A more certain answer is expected from study of larger systems.

The work planned for the future emerges as a logical continuation of the work already begun. We intend to extend this work to larger, more complicated and more realistic systems.

References

[1] P. Hohenberg and W. Kohn, Phys.Rev.**136**, B 864 (1964); W. Kohn and L.J. Sham, Phys.Rev.**140**,A 1133 (1965)

[2] See, for instance, Theory of the Inhomogeneous Electron Gas, ed. by S.Lundquist and N.H. March (Plenum, New york, 1983)

[3] S. Kirkpatrick, C.D. Gelatt, Jr. and M.P. Vecchi, Science **220** 671 (1983)

[4] N. Metropolis, A. and M. Rosenbluth, A. and E Teller, J.Chem. Phys.**21**, 1087 (1953)

[5] R. Car and M. Parrinello, Phys.Rev.Lett **55**, 2471 (1985)

[6] A. Williams and J. Soler, in abstracts in section FO, Bull.Am.Phys.Soc**32**, 562 (1987)

[7] R. Car, M. Parrinello, and W. Andreoni, in Proc. 1st NEC Symp. on Fundamental Approach to New Material Phases, ed. by S. Sugano and S. Ohnishi (Springer, Berlin, 1987), p.134

[8] R. Benedek, B.I. Min, and J. Garner, Preprint

[9] Metastable electronic configurations for fixed ionic positions cannot, of course, be ruled out, but are expected to be rare.

[10] L. Verlet, Phys.Rev. **159**, 98 (1967)

[11] Numerical Receips, by W.H. Press, B.P. Flannery, S.A. Teukolsky, and W.T. Vetterling (Cambridge University, 1986), p.301; L.A.Hageman and D.M.Young, in Applied Iterative Methods, Computer Science and Applied Mathematics (Academic, New York, 1981), p.138

[12] I. Štich, R. Car, and M. Parrinello, to be published

[13] D.J. Chadi and M.L. Cohen, Phys.Rev. B8, 5747 (1973)

[14] M.C. Payne, J.D. Joannopoulos, D.C. Allan, M.P. Teter, and D.M. Vanderbilt, Phys.Rev.Lett.**56**, 2656 (1986)

[15] E.R. Davidson, in Methods in Computational Molecular Physics, ed. by G.H.F. Diercksen and S. Wilson (NATO ASI 1979), vol. 113, p.95

[16] D.R. Hamman, M. Schlueter, and C. Chiang, Phys.Rev.Lett. **43**, 1494 (1979)

[17] J.P.Perdew and A. Zunger, Phys.Rev. B**23**, 5048 (1981)

[18] G. Galli and M. Marinelli, private communication

[19] G.B. Bachelet, D.R. Hamman, and M. Schlueter, Phys.Rev. B**26**, 4199 (1982)

[20] M.C. Payne, to be published

[21] P. Madden and M. Sprik, private communication

[22] See, for instance, a review by N. Rivier, Adv.in Phys.**34**, 95 (1987)

[23] G.A.N. Connell and R.J. Temkin, Phys.Rev. B**9**, 5323 (1974)

[24] D.C. Mattis, Phys.Lett. **56A**, 421 (1976)

[25] N. Rivier, Phil.Mag. A**40**, 859 (1979)

[26] G. Toulouse and M. Kleman, J.Phys.Lett (Paris) **37**, 449 (1976)

[27] D. Mermin, Rev.Mod.Phys. **51**, 591 (1979)

[28] G. Toulouse, Phys.Rep. **49**, 267 (1979)

[29] N. Rivier and D.M. Duffy, in Critical Phenomena vol.9, ed. by J. Della-Dora, J. Demongeot, and B. Lacolle (Springer, Berlin, 1981), p.132

[30] See, for instance, Amorphous Solids. Low temperature Properties Topics in Current Physics, ed. by W.A. Philips (Springer, Berlin, 1981)

[31] N. Rivier and D.M. Duffy, J.Physique (Paris) **43**, 293 (1982)

[32] N. Rivier, in Topological Disorder in Condensed Matter, ed. by F. Yonezawa and T. Ninomiya (Springer, Berlin, 1983), p.14

[33] M.H. Cohen, in Topological Disorder in Condensed Matter, ed. by F. Yonezawa and T. Ninomiya (Springer, Berlin, 1983), p.133

[34] F. Yonezawa and M.H. Cohen, in Fundamental Physics of Amorphous Semiconductors, (Springer, Berlin, 1981), vol 25, p.119

[35] D.Weaire, Phys.Rev.Lett. **26**, 1541 (1971)

[36] L. Ley, S. Kawalczyk, R. Pollak, and D.A. Shirly, Phys.Rev.Lett. **29**, 1088 (1972)

[37] S.T. Pantelides, Phy.Rev.Lett. **57**, 2979 (1986)

[38] R. Car and M. Parrinello, in Proc. 18th Int.Conf.Phys.Semicond. Stockholm 1986, ed. by O. Engstrom (World Scientific Publ. Co., Singapore, 1987), p.1165

[39] R. Car and M. Parrinello, to be published

[40] T.M. Hayes and J.W. Allen, J.Non-Cryst.Solids **77**, 57 (1985)

[41] J.C. Phillips, J.C. Bean, B.A. Wilson, and A. Ourmazd , Nature **335**, 121 (1987)

[42] See, for instance, D. Henderson, J.Non-Cryst.Solids **16** , 317 (1974); D.L. Evans, M.P. Teter, and N.F. Borreli, J.Non-Cryst.Solids **17** , 245 (1975); D. Beeman and B.L. Bobbs, Phys.Rev. **B12**, 1399 (1975); D.E. Polk and D.S. Boudereaux, Phys.Rev.Lett. **31**, 92 (1973); P. Steinhardt, R.A. Alben, and D. Weaire, J.Non-Cryst.Solids **15** , 199 (1974); F. Wooten, K. Winer, and D. Weaire, Phys.Rev.Lett. **54**, 1392 (1985); F. Wooten and D. Weaire, J.Non-Cryst.Solids **64**, 325 (1984); K. Winer, Phys. Rev. **B35**, 2366 (1987)

[43] R. Zallen, in Fluctuation Phenomena, ed. by E.W. Montroll and J.L. Lebowitz (North Holland, 1979), ch.3

[44] S.V. King, Nature, 1113 (1967)

[45] J.H. Etherington, A.C. Wright, J.T. Wenzel, J.C. Dore , J.Clarke, R.N. Sinclair, J.Non-Cryst.Solids **48**, 265 (1982)

[46] I.Štich, R. Car, and M. Parrinello, to be published

[47] F.H. Stillinger and T.A. Weber, Phys.Rev. B**31**,5262 (1985)

[48] J.Q. Broughton and P.B. allen, in Computer Based Microscopic Description of the Structure and Properties of Materials, ed. by J.Q. Broughton, W. Krakow, and S.T. Pantelides (MRS, Boston, 1986)

[49] F.H. Stillinger and T.A.Weber, Science **225**, 983 (1984)

[50] R.A. La Violette and F.H. Stillinger, Phys.Rev. B**35** , 5446 (1987)